Ore Geology Reviews 120 (2020) 103452

Contents lists available at ScienceDirect

Ore Geology Reviews

journal homepage: www.elsevier.com/locate/oregeorev

Geology, mineralization, and fluid inclusion characteristics of the Agylki reduced tungsten (W-Cu-Au-Bi) skarn deposit, Verkhoyansk fold-and-thrust belt, Eastern Siberia: Tungsten deposit in a gold-dominant metallogenic province

Serguei G. Soloviev[a,*], Sergey G. Kryazhev[b], Svetlana S. Dvurechenskaya[b]

[a] Institute of Geology of Ore Deposits, Petrography, Mineralogy and Geochemistry (IGEM), Russian Academy of Sciences, 35 Staromonetny Per., Moscow 109017, Russia
[b] Central Research Institute of Geological Prospecting for Base and Precious Metals (TsNIGRI), 1-129 Warshawskoe Chaussee, Moscow 117545, Russia

ARTICLE INFO

Keywords:
Reduced skarn
Tungsten
Gold
Fluid inclusions
Verkhoyansk orogenic belt

ABSTRACT

The Agylki deposit is a large (> 100 Kt WO_3, possibly underexplored) and high-grade (average 1.46% WO_3, 2.79% Cu, 0.5 g/t Au, and 0.03–0.04% Bi) reduced W skarn deposit situated in the Verkhoyansk fold-and-thrust belt, the latter formed after a passive continental margin, part of the Verkhoyansk-Kolyma gold-dominant metallogenic province. The belt comprises intrusion-related Au mineralization and roughly parallels the other main metallogenic belts of the region hosting numerous gold (Au, Au-Bi, Au-Sb, etc.) and W-Sn deposits. The deposit could be part of a broader regional-scale magmatic-hydrothermal system comprising nearly coeval intrusion-related reduced W skarn deposits and vein/stockwork Au(± W) deposits. The deposit is related to a swarm of Late Jurassic-Early Cretaceous monzodiorite-porphyry, granodiorite- and granite-porphyry dikes that intrude a Triassic terrigenous sequence. The dikes comprise weakly reduced-weakly oxidized (ilmenite-titanite-bearing), high- to medium-K calc-alkaline, metaluminous to weakly peraluminous, I-type granitoid rocks.

The deposit is represented by a single lenticular flat-lying to shallow-dipping mineralized zone that was formed by the replacement of a limestone horizon. This may correspond to a distal level in an integrated structural model of W skarn deposits that occurs well above causative pluton. The deposit bears signatures of reduced W skarn deposits, with dominant pyroxene skarn containing pyrrhotite and scheelite. Propylitic alteration assemblages (amphibole-epidote-chlorite-calcite-quartz with abundant pyrrhotite, scheelite and minor chalcopyrite) overprint skarn and are in turn overprinted by zones of phyllic alteration (quartz-sericite-Fe-carbonate) comprising abundant apatite and arsenopyrite followed by scheelite, chalcopyrite and other sulfides as well as Bi, Te and Au minerals.

Fluid inclusions data indicate formation of retrograde (mainly pyroxene-quartz-amphibole) skarn from aqueous, dominantly magnesian-sodic-chloride, moderate-salinity (14.0–17.3 wt% NaCl-eq.), high pressure (1.4 ± 0.2 kbars), moderately-hot (~400–500 °C) fluid. Propylitic alteration assemblages were formed from homogenous, low-carbonic, lower salinity (8.8–13.7 wt% NaCl-eq.), lower pressure (1.1–0.8 kbars) and lower temperature (~300–400 °C) Ca-enriched fluid. Early phyllic alteration assemblages were formed from a boiling fluid, with separation of carbonic-rich (particularly methane-enriched) gaseous fluid and coexisting low-carbonic aqueous fluid at ~320–280 °C and ~0.9 ± 0.1 kbar. Late phyllic alteration assemblages were formed from homogenous, low-carbonic, moderate-salinity (14.0–17.8 wt% NaCl-eq.) low-temperature (250–200 °C) fluid.

1. Introduction

The Verkhoyansk-Kolyma system of orogenic belts is well known for its gold endowment and is primarily distinguished as one of the largest Au metallogenic provinces in the Eastern Siberia, where dominantly orogenic-type to reduced intrusion-related Au deposits, locally with associated As, Sb, Bi mineralization, are widespread, including a number of the world-class examples (Goryachev, 1998, 1999; Yakubchuk, 2009; Bortnikov et al., 2010; Seltmann et al., 2010; Goldfarb et al., 2014; Goryachev and Pirajno, 2014; Fridovsky, 2002,

* Corresponding author.
E-mail address: serguei07@hotmail.com (S.G. Soloviev).

https://doi.org/10.1016/j.oregeorev.2020.103452
Received 7 December 2019; Received in revised form 18 February 2020; Accepted 3 March 2020
Available online 05 March 2020
0169-1368/

2018; Vikent'eva et al., 2018). There are also large tin deposits in this province including tin-polymetallic (tin-sulfide) and W-Sn deposits of the greisen to quartz stockwork types, as well as large Ag-Sb deposits (e.g., Seltmann et al., 2010; Voroshin et al., 2014). Less is known about W skarn deposits in this province, although some of them contain significant W resources.

In particular, the Agylki W skarn deposit situated in the Verkhoyansk fold-and-thrust belt hosts significant W resources, principally in a single large "stratabound" orebody containing indicated resources ~94,000 t WO_3 with average grade of 1.27% WO_3 (0.4% WO_3 cut-off), plus inferred resources ~35 Kt WO_3. The tungsten orebody also contains on average 2.72% Cu, 16.2 g/t Ag, 0.046% Bi, 21 g/t Te and 54 g/t Se, and its part – 1.38 g/t Au (0.6 g/t Au cut-off); this corresponds to the resources of 193 Kt Cu, ~4 t Au, 47 t Ag, 3300 t Bi, 150 t Te and 386 t Se (Protopopov et al., 2016). Additional resources found in mineralized stockworks below and above the "stratabound" tungsten orebody were not evaluated. The deposit was discovered in 1954–1955 by tracing alluvial scheelite anomalies toward surface outcrops of mineralized zones, explored in 1956–1976 by trenching and drilling, and considered as a "reserve deposit" since, with no mining operations occurred due to the remote location and lack of infrastructure. The deposit was studied by G.M. Bilinkis, I.I. Stegnach., D.I. Larin, D.A. Dorofeev, V.A. Amuzinsky, B.L. Flerov, V.I. Naiborodin and others in 1954–1979, mostly in terms of structural setting and mineralogy of mineralized zones, and most recently by Gvozdev (2002, 2010). The present paper, focused on new petrologic, mineralogy and fluid inclusion data, is aimed at revealing conditions of the deposit formation, highlighting its regional metallogenic role, comparing with other deposits of this type globally, and expanding an integrated genetic model of reduced W skarn deposits.

2. Regional tectonic and metallogenic setting

The Verkhoyansk-Kolyma system of orogenic tectonic and metallogenic belts is part of the Verkhoyansk-Chukotka orogenic province of Mesozoic-Cenozoic collages comprising Precambrian cratonic terranes (Asian cratonic fragments) and accreted late Paleozoic to Cenozoic turbidite to island arc terranes (Fig. 1; Yakubchuk, 2009; Nokleberg et al., 1998). Collisional processes in the Verkhoyansk-Kolyma system occurred in the Late Jurassic-Valanginian due to the closure of the Oimyakon paleoocean and subsequent collision of the Siberian craton with Kolyma-Omolon and Okhotsk microcontinents or superterrains (Parfenov, 1995; Parfenov and Kuzmin, 2001; Goryachev and Pirajno, 2014). According to Fridovsky (2018), the early and late collisional stages can be distinguished, which correspond to the Late Jurassic-Berriasian and Berriasian-Valanginian, respectively. The early-collisional stage is related to the early deformations of the outer zone of the Verkhoyansk-Kolyma system, whereas the late-collisional stage is associated with the culmination of the craton-microcontinent collision due to the westward migration of the most intense deformations. The late-collisional stage was also characterized by intense granitoid magmatism. The Verkhoyansk-Kolyma orogenic system is characterized by intense Au mineralization including numerous large Au deposits, principally of the orogenic to reduced intrusion-related classes (Goryachev, 1998, 1999; Yakubchuk, 2009; Seltmann et al., 2010; Goldfarb et al., 2014; Goryachev and Pirajno, 2014; Vikent'eva et al., 2018).

The Agylki deposit is situated in the Verkhoyansk fold-and-thrust belt, which occurs in the southwestern part of the Verkhoyansk-Kolyma system most proximal to the Siberian craton and extends for almost 2000 km along its margin (Fig. 1; Goryachev et al., 2018). This belt was formed over a passive cratonic margin and overlies a metamorphic Achaean-Proterozoic basement. Since the late Precambrian and almost to the Late Jurassic, the territory corresponded to a passive continental margin, with episodic Middle-Late Devonian rifting. Consistently, it is composed of sandstone–siltstone, mainly deltaic to shallow shelf, turbiditic, less typically flysh to black shale sequences. These rocks were deposited during the Carboniferous-Jurassic, attain a cumulative thickness up to 15 km, and were folded and thrusted during the Late Jurassic to Early Cretaceous (Berriassian-Valanginian) (Parfenov, 1995).

To the north-east, the Verkhoyansk thrust-and-fold belt is bordered by the Yana-Kolyma belt of granitoid intrusions that were emplaced along a suture zone between the Verkhoyansk deformed passive margin of the Siberian craton and the island arc terranes (e.g., Yakubchuk, 2009). The belt comprises two major types of the Late Jurassic-Cretaceous granitoid intrusions, namely, (1) small diorite-granodiorite intrusions (stocks, dikes), and (2) large (batholitic) granodiorite-granite to granite-leucogranite plutons. The former are characterized by deeper magmatic sources, possibly in the upper mantle or lower crust, whereas the latter are most distinctly related to crustal sources, with substantial input from melting of terrigenous sedimentary rocks (Goryachev, 1999). The group of small diorite-granodiorite intrusions includes those referred to as the Nera-Bokhapchin and/or Basugunyin dike suites that comprise the most numerous dikes, particularly in the districts with the most abundant Au mineralization (e.g., Volkov et al., 2010). Akinin et al. (2009) dated diorite-granodiorite dikes of the Nera-Bokhapchin suite at 153 to 150 ± 2 Ma, and similar dikes of the Basugunyin suite - at 158.5 ± 1.4 Ma (U-Pb method on zircons). The large granodiorite-granite to granite-leucogranite plutons are usually referred to as the Kolyma plutonic suite, with the most of these plutons dated at ~150 Ma (Protopopov et al., 2016), which is consistently younger than the age of the small stock/dike suites occurring in the same locations. The Late Jurassic-Cretaceous granitoid suites, both these of small stocks/dikes and large plutons, are accompanied by Au and Au-Sb deposits (Maltan, Sarylakh, Sentachan, etc.; e.g., Bortnikov et al., 2010; Vikent'eva et al., 2018). Some granitoid plutons are also accompanied by W-Sn deposits, thus constituting regional intrusion-related Au-Sn-W metallogenic system (Goryachev, 1999; Goryachev and Pirajno, 2014; Voroshin et al., 2014; cf. Thompson et al., 1999).

A younger suite of small intrusions and dikes occurs in the transverse northeast-trending, typically concealed belts (Fig. 2) that were likely formed due to an extensional event (Layer et al., 2001). These intrusions comprise a broad variety of rocks including lamprophyre, diorite, granodiorite, and granite, and are dated at 136 to ~100 Ma (Ar-Ar method), with the age decreasing toward the south-west (Prokopiev et al., 2010). These transverse, northeast-trending belts of granitoid intrusions are characterized by dominant Ag-polymetallic deposits (Prognoz, Mangazeya, etc.), typically together with Sn-polymetallic (Sn-Pb-Zn) mineralization (Fig. 2).

3. District geology and mineralization

The mineralized district comprising the Agylki deposit is situated in the Tompon metallogenic zone that extends for 300–500 km roughly parallel to the outer margin of the Verkhoyansk belt (Fig. 2; Protopopov et al., 2016). This zone comprises Au and Au-Sb occurrences (Amyzinsky, 1974) and is defined by generally east–west to west-northwest-striking faults that can be traced from the South Verkhoyansk metallogenic zone to the southeast. As a result, it can be speculated that the Tompon zone represents a west-northwestern extension of the north–south-trending South Verkhoyansk metallogenic zone comprising large Au deposits with significant Sb, As, Bi and minor W (scheelite) mineralization (Nezhdaninskoe, etc.; Bortnikov et al., 1998; Fridovsky, 2002, 2018).

The Au and Au-Sb mineralization in the Tompon zone is represented by auriferous quartz-sulfide to quartz-sulfide-scheelite veins and stockworks, with dominant arsenopyrite and pyrrhotite accompanied by pyrite, Bi minerals, sphalerite, galena and stibnite (Amuzinsky, 1974). The mineralization is closely associated with the Late Jurassic to Early Cretaceous calc-alkaline dioritic to granitoid stocks and east–west-striking dikes, which in the Tompon zone are traditionally

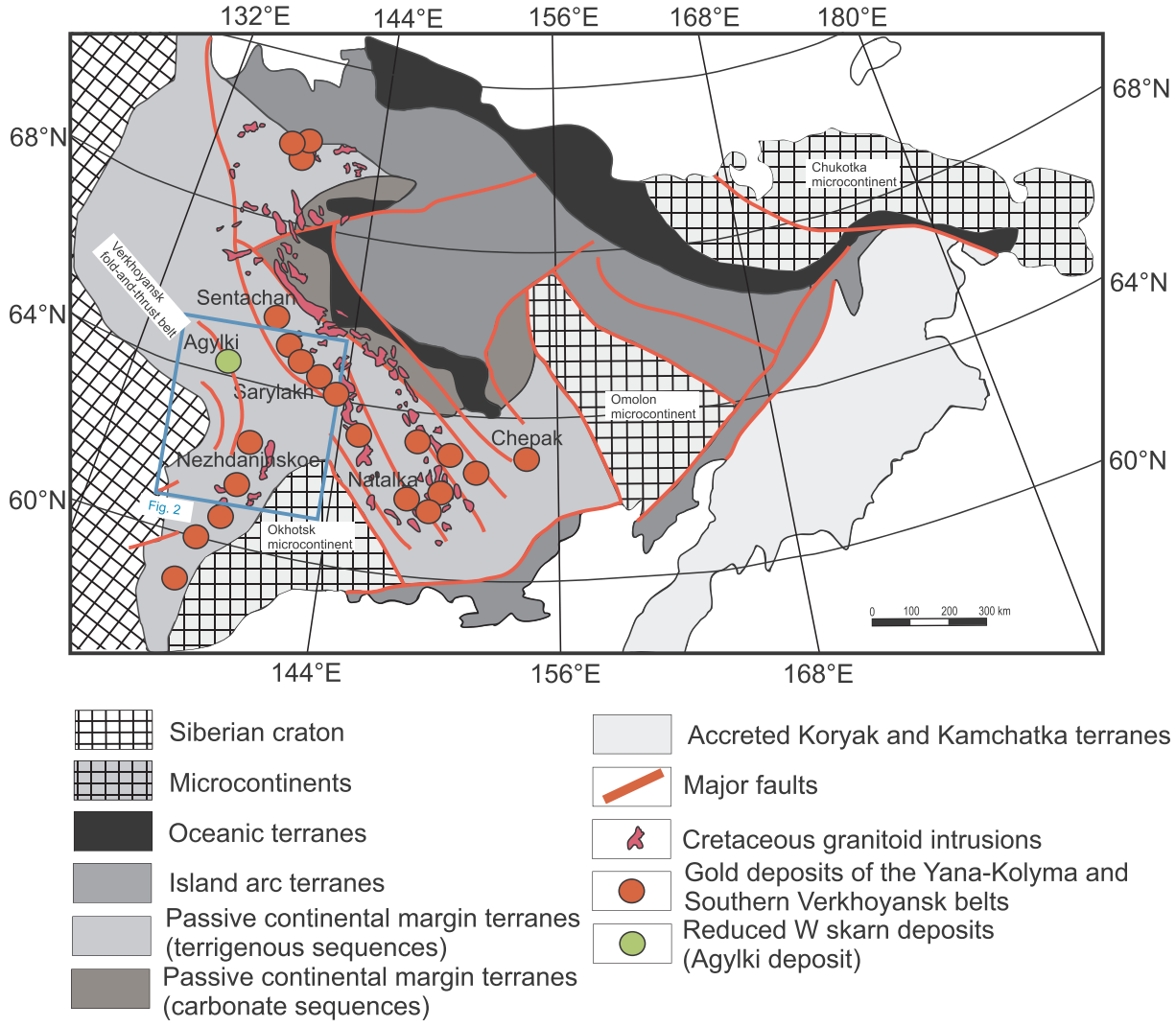

Fig. 1. Regional tectonic setting of the Agylki W skarn deposit and some Au deposits in the Verkhoyansk-Chukotka orogenic province (modified after Goryachev et al., 2018; Goryachev, 1998, 1999; Parfenov, 1995; Parfenov and Kuzmin, 2001).

assigned to the Basugunyin and/or the Nera-Bokhapchin dike suites (e.g., Flerov et al., 1974), i.e., the igneous suites distinguished in the Yana-Kolyma magmatic and metallogenic belt situated far north. To address this ambiguity, Protopopov et al. (2016) distinguished the separate Uemlyakh stock and dike suite, which, however, currently appears to be too broad, as it includes a younger group of high-K calc-alkaline granitic intrusions accompanied by Sn-W mineralization. Larger granitoid stocks found north and northeast of the Agylki deposit and accompanied by Sn-W mineralization are younger (130 Ma to 116–109 Ma by K-Ar method; Flerov et al., 1974; Protopopov et al., 2016) than monzodiorite-porphyry and granitoid dikes accompanied by W and Au mineralization. This younger Sn-W mineralization is represented by quartz-tourmaline veins and stockworks with cassiterite and wolframite.

4. Deposit geology

The Agylki deposit is associated with a large swarm of generally east–west-trending, subvertical granitoid dikes that intrude folded Triassic terrigenous rocks comprising grey sandstone, siltstone, less commonly conglomerate and limestone (Fig. 3). The Lower Triassic rocks underlie most of the deposit area; their cumulative thickness is estimated at > 850 m. At the bottom of the Lower Triassic sequence, a limestone horizon some 3–5 m thick is present; it comprises numerous small lenses and thin lenticular layers of siltstone. The Lower Triassic rocks are tectonically overlain by a Middle Triassic (?) sequence occurring in the eastern part of the deposit area and dominated by calciferous sandstone with minor siltstone and conglomerate horizons. The Lower Triassic sedimentary rocks form a gently to moderately steeply dipping anticline, with its limbs complicated by smaller folds. The bedding has a shallow dip in the fold closure (~8-15°) and in its western limb but becomes steeper (up to 25-30°) in the eastern limb and to a depth. The Lower Triassic siltstone unit comprises a thin grayish-white limestone horizon that outlines the fold closure and was traced downdip for > 800 m along the limbs (Fig. 3). Thickness of this horizon slightly increases in closures of smaller (parasitic) anticlines complicating the major fold. The limestone horizon comprises thin (0.1–10 cm) siltstone layers (5–8 layers per 1 m of the thickness). Siltstone was converted into biotite (amphibole-biotite) hornfels over the deposit area.

The anticline is crosscut by numerous paralleling, typically east–west-striking subvertical (to south-dipping at 70-85°) dikes, which are part of a much larger dike field extending for ~5 km to the west of the deposit area. The dikes vary in thickness (from 1.5 to 2 m to 20 m) and composition (lamprophyre, monzodiorite to quartz monzodiorite-porphyry, granodiorite-porphyry, granite-porphyry). It appears that the number of dikes and their thickness increases with depth. The thickest (~20 m) granodiorite-porphyry dike is situated in the central part of

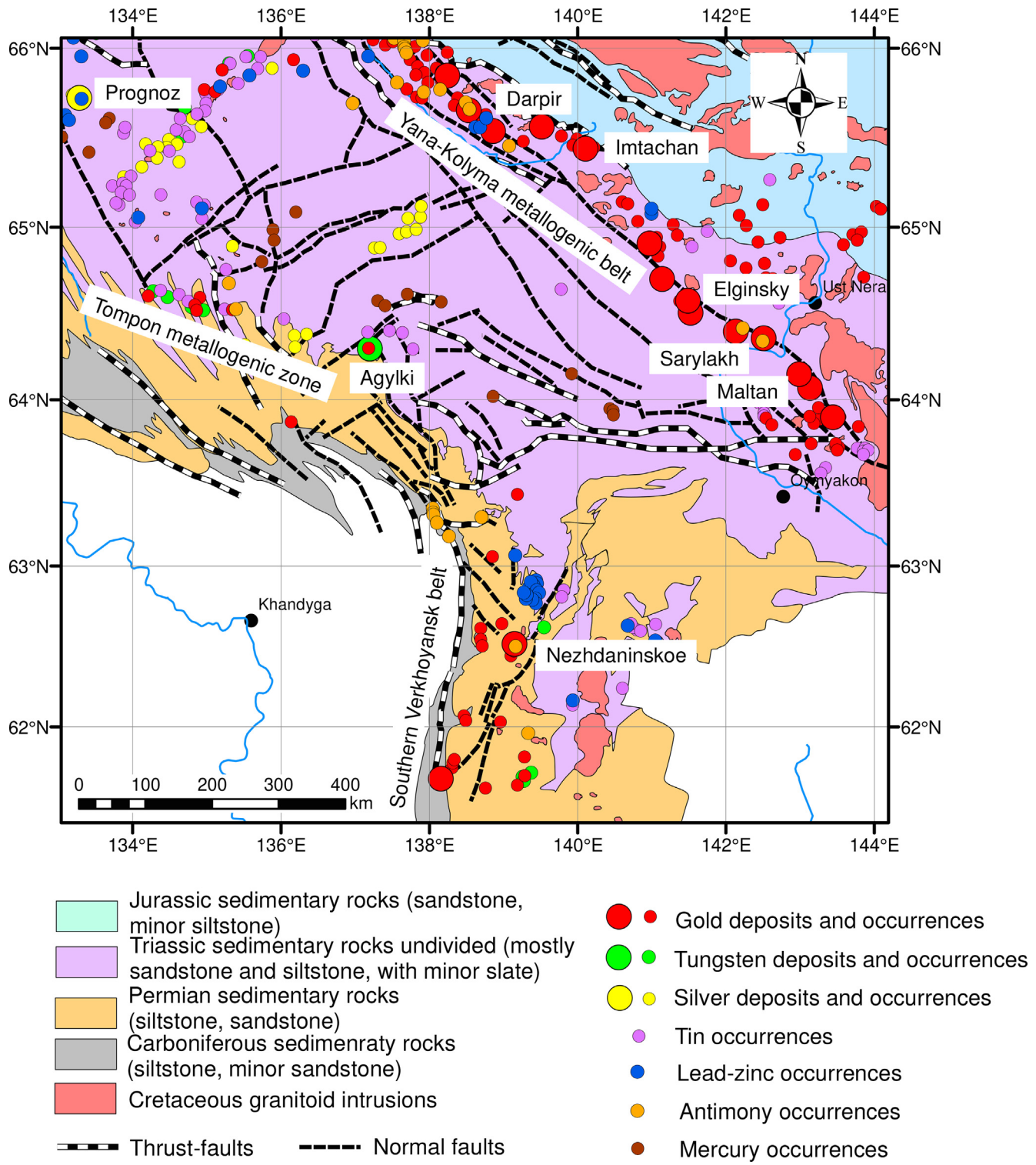

Fig. 2. Geological map of the southern part of the Verkhoyansk fold-and-thrust belt and adjacent territories showing location of the Agylki deposit and other (Au, Sn, Sb, Ag, Pb-Zn, etc.) deposits and occurrences (modified after Protopopov et al., 2016).

the dike field. A biotite hornfelsing halo is present in the center of the deposit area. Based on these signatures, a larger granitoid intrusion is suggested at depth (Bilinkis, 1961). Flerov et al. (1974) reported a very Late Jurassic to Early Cretaceous whole rock radiologic K-Ar age of these granitoid dikes (145–143 Ma) and assigned the dikes to the Basugunyin dike suite. Lamprophyre dikes mapped in the southern part of the deposit area were dated at 190 ± 17 Ma (K-Ar method; Flerov et al., 1974) and can represent an older igneous suite.

The deposit is represented by the only scheelite-sulfide orebody found in the western part of the anticline and formed by replacement of the limestone layer by skarn and post-skarn mineral assemblages (Fig. 3). As a result, the orebody follows this lenticular limestone horizon and is generally lenticular flat-lying to gently-dipping; it was traced for ~1200 m on the surface by trenching and surface outcrops, for ~500–860 m downdip by drilling, and varies in thickness from 2.1 to 8.8 m averaging 4.3 m (Bilinkis, 1961; Dorofeev, 1961). The

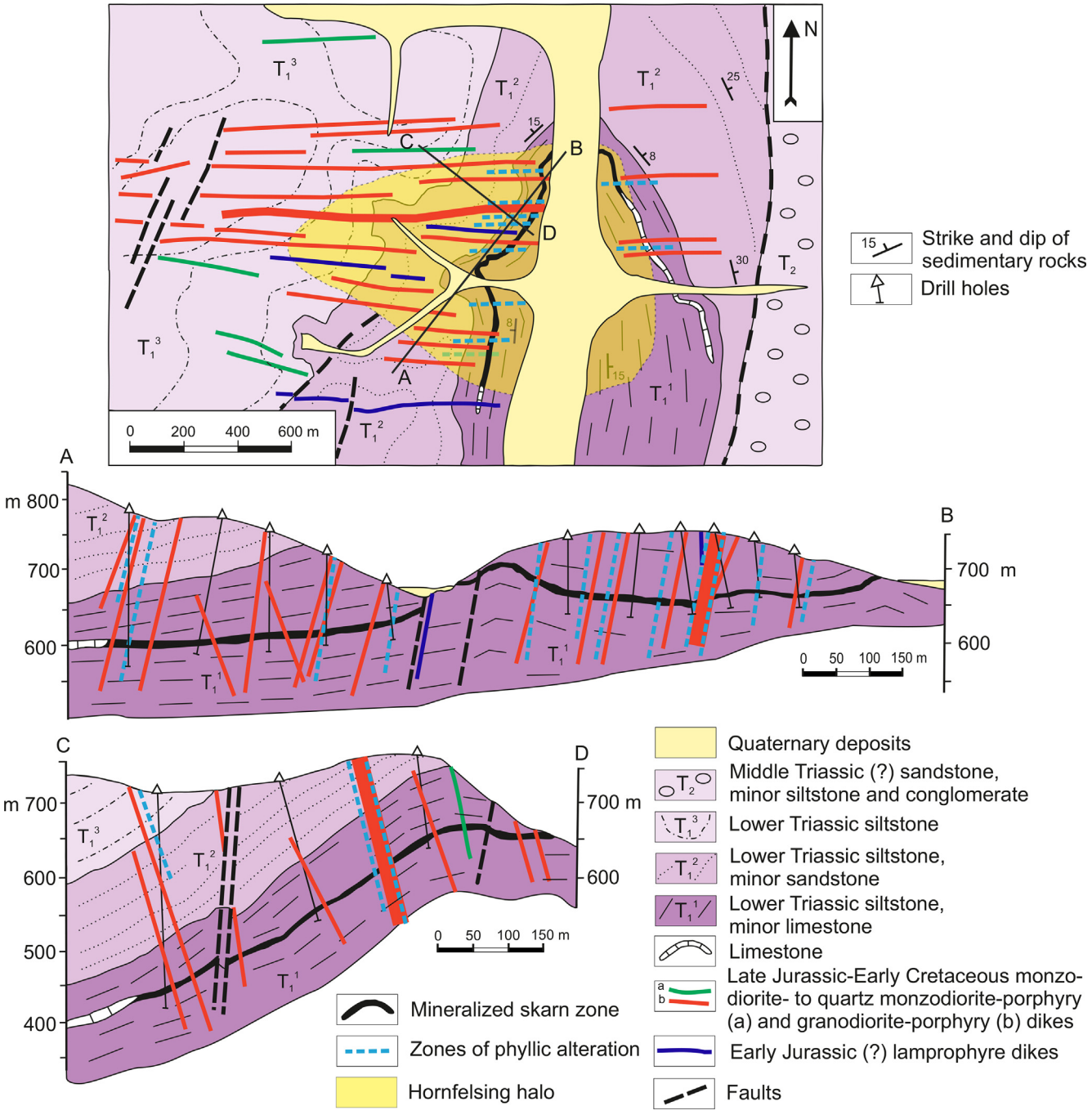

Fig. 3. Geological map and sections of the Agylki deposit (modified after Bilinkis, 1961; Dorofeev, 1961; Flerov et al., 1974; Gvozdev, 2002, 2010).

thickness locally increases near granitoid dike contacts intersecting the orebody. The mineralization overprints and replaces skarn and is associated with narrower, typically concordant (flat-lying to gentle-dipping) zones of post-skarn quartz-amphibole-chlorite (propylitic) alteration as well as with typically discordant (subvertical) linear zones of quartz-sericite-carbonate (phyllic) alteration assemblages bearing scheelite and sulfides. Together, an overprint of skarn by these post-skarn alteration assemblages causes almost entire replacement of skarn minerals and the overall high-grade average metal (W, Cu, Bi) contents associated with the intervals of massive to densely-disseminated (pyrrhotite- and/or chalcopyrite-dominant) sulfide mineralization. Tungsten grades vary from 0.1 to 5.69% WO_3 averaging 1.27% WO_3 (Bilinkis, 1961). Scheelite in high-grade intervals occurs as dense dissemination, common large (several centimeters across) patches of grains, and as thick short veinlets. The mineralized skarn zone splits into disconnected lenses downdip and in the eastern part of the anticline.

In more detail, the metal grade distribution shows more complicated pattern (Fig. 4). It appears that granitoid dikes intersecting the flat-lying skarn zone control the intervals of the highest metal values, locally exceeding 2% WO_3 and 2–3% Cu, as these intervals in zones of phyllic alteration overprinting skarns occur most proximal to these dikes. These high-grade zones (or “ore shoots”) plunge gently to the west, together with the general dip of the skarn zone. In addition, the highest metal grades tend to occur in the central part of the orebody that is coincident with the anticline closure and its immediate surroundings, whereas the grades gradually decrease toward the edges of the orebody, i.e., toward its deeper parts. It further appears that these

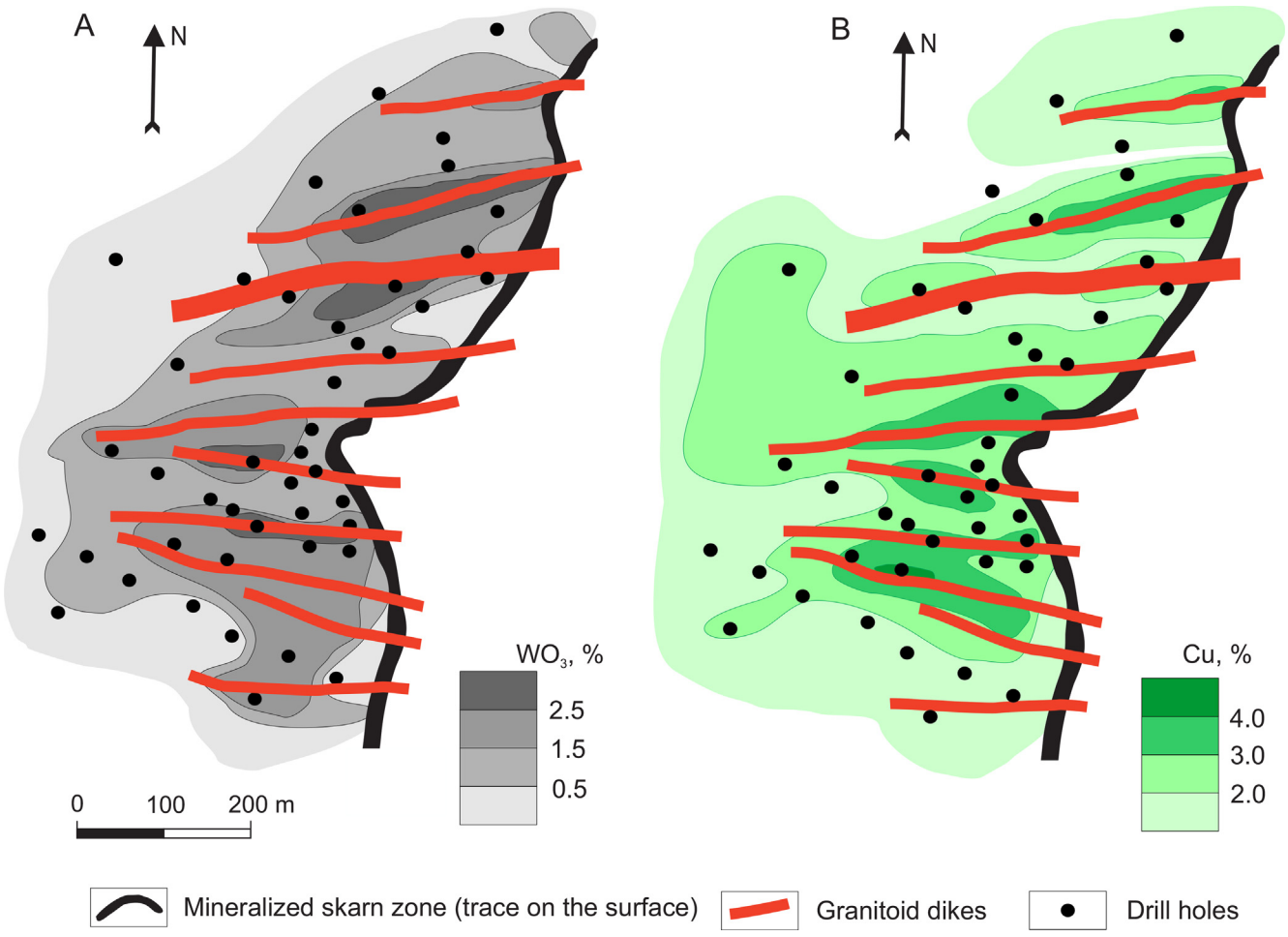

Fig. 4. Distribution of Au (A) and Cu (B) grades in horizontal projection of the mineralized zone at the Agylki deposit (modified after Bilinkis, 1961; Flerov et al., 1974).

deeper parts of the orebody comprise less intense propylitic and phyllic alteration overprinting skarn, thus emphasizing the role of superposition of various hydrothermal alteration assemblages in establishing higher metal grades.

In addition to the main flat-lying to gently-dipping orebody, there are several linear stockworks up to 20 m wide, typically subvertical, that are traced both above (up to 80–100 m upward) and below the main orebody. These stockworks representing mainly phyllic alteration assemblages (quartz-sericite to quartz-sericite-carbonate) comprise veined and disseminated mineralization, mostly arsenopyrite, pyrrhotite, chalcopyrite, pyrite, galena, sphalerite, in total attaining 5–10 vol%, and minor scheelite. Some intervals (up to 3 m) bear elevated Bi (0.5–1%) and Ag (90–110 g/t) contents (Protopopov et al., 2016).

5. Analytical methods

Description of analytical methods is given in the Electronic Supplement.

6. Igneous rocks

The deposit area comprises numerous dikes of mafic and granitic rocks (Table 1), which are assigned to both the Late Jurassic-Early Cretaceous plutonic suite and an older (Early Jurassic?) suite. The Late Jurassic-Early Cretaceous rocks comprise monzodiorite- to quartz monzodiorite-porphyry, granodiorite-porphyry and granite-porphyry, whereas older (Early Jurassic?) rocks are represented by lamprophyre (camptonite to spessartite; Flerov et al., 1974; Gvozdev, 2010) dikes. Whereas relatively fresh lamprophyre dike occurs at the southern flank of the deposit, strongly altered lamprophyre dikes are present within the main dike swarm immediately west of the mineralized zone. Bilinkis (1961) reported lamprophyre xenoliths in granodiorite-porphyry dikes. The monzodiorite- to quartz monzodiorite-porphyry forms several dikes and is a weakly-porphyritic rock, with small (~1 mm) plagioclase phenocrysts (zoned from labradorite-bytownite with 70–80 mol.% anorthite in the core to andesine with 40–50 mol.% anorthite in the rims); it contains both amphibole and biotite.

Granodiorite-porphyry forms the majority of the dikes including the largest (20 m thick) dike. It is a porphyritic rock, with large (up to 5 mm) plagioclase phenocrysts (zoned from andesine-labradorite with 50–60 mol.% anorthite in the core, locally strongly resorbed, to andesine with 30–40 mol.% anorthite in the rims) locally forming glomeroporphyry aggregates. Biotite and locally rounded (also corroded and embayed) quartz phenocrysts are smaller and less common. The rock contains no amphibole and is composed of brown biotite (10–15 vol%), plagioclase (40–50 vol%), K-feldspar (15–20 vol%) and quartz (20–25 vol%). Graphic and micropegmatitic quartz-feldspar intergrowths as well as microvugs filled with quartz, feldspars, and locally ilmenite and calcite, are common. Granite-porphyry dikes are rare; this fine-grained and leucocratic, locally aplitic, rock contains minor brown biotite (3–5 vol%). Accessory minerals in the igneous rocks include zircon, apatite, ilmenite, allanite, titanite, and rutile. Sagenite is locally present in biotite.

On the total alkalis vs. SiO_2 diagram (Fig. 5A), monzodiorite- to quartz monzodiorite-porphyry lies in the midalkaline field, whereas

Table 1
Major petrographic features of igneous rocks from the Agylki deposit.

Intrusion phase	Rocks	Petrography
(An older suite?)	Lamprophyre (camptonite and spessartite)	Mafic (dark greenish-grey) porphyritic rock with greenish-brown amphibole phenocrysts, minor (in camptonite) to abundant (in spessartite) dark-brown biotite phenocrysts and minor olivine or pyroxene (augite to Ti-augite?) phenocrysts, the latter revealed by talc-carbonate to biotite-chlorite-titanite pseudomorphs. The groundmass is composed of brown to reddish-brown amphibole, plagioclase (labradorite with 55–65 mol.% anorthite) and dark-brown biotite. In total, the rock contains 30–40 vol% amphibole (in camptonite) to 5–10 vol% amphibole (in spessartite), 10–20 vol% biotite (in camptonite) to 25–30 vol% biotite (in spessartite), 1–3 vol% olivine or pyroxene, 60–70 vol% plagioclase, and 0–10 vol% K-feldspar (orthoclase). Microvugs filled with calcite are locally present. Accessory minerals include ilmenite, acicular apatite, titanite, and zircon.
1	Monzodiorite- to quartz monzodiorite-porphyry	Fine- to medium-grained weakly-porphyritic mesocratic (greenish-grey to pinkish-grey) rock composed of brownish-green amphibole (3–5 vol%), dark-brown biotite (20–30 vol%), plagioclase (50–60 vol%), locally K-feldspar (orthoclase and microcline) (5–15 vol%), and quartz (0–10 vol%). Phenocrysts are represented by zoned plagioclase (from bytownite with 70–75 mol.% anorthite in the core to andesine-labradorite with 50–60 mol.% anorthite in the rims) and are typically small (< 1 mm); phenocrysts form 15–25 vol% of the rock. Plagioclase in the groundmass is andesine with 50–57 mol.% anorthite. Accessory minerals – apatite, zircon, titanite, and ilmenite.
2	Granodiorite-porphyry	Medium-grained porphyritic mesocratic (greenish-grey to light-grey) rock composed of dark-brown biotite (10–15 vol%), plagioclase (40–50 vol%), K-feldspar (orthoclase and microcline) (15–20 vol%), and quartz (20–25 vol%). Phenocrysts form 20–50 vol% of the rock, are up to 5 mm across, and are composed of zoned plagioclase (from andesine-labradorite with 50–60 mol.% anorthite in the core, locally strongly resorbed, to andesine with 30–40 mol.% anorthite in the rims). Glomeroporphyry aggregates are common. The groundmass is composed of fine-grained plagioclase (andesine-oligoclase), K-feldspar, quartz and biotite. Graphical and micropegmatitic textures are common. Microvugs filled by quartz, feldspars, and locally ilmenite and calcite are present. Accessory minerals include apatite, ilmenite, titanite, allanite, zircon, monazite, rutile, and scheelite. A more mafic and finer-grained rock petrographically similar to monzodiorite- to quartz monzodiorite-porphyry forms an outer rim (with sharp contacts) in larger granodiorite-porphyry dikes; this narrow endocontact zone may represent a marginal zone of early crystallization (i.e., quenched facies) of granodiorite-porphyry.
3	Granite-porphyry	Fine-grained porphyritic to aplitic leucocratic (light-grey to white) rock composed of brown biotite (3–5 vol%), plagioclase (30–35 vol%), K-feldspar (orthoclase and microcline) (20–25 vol%), and quartz (30–35 vol%). Phenocrysts of plagioclase (andesine-oligoclase), quartz and minor K-feldspar are present, whereas the groundmass is composed of K-feldspar and quartz. Mirmekites and graphic intergrowths of quartz and feldspars are common, and spherolitic texture is locally present. Accessory minerals include ilmenite, titanite, apatite, zircon, and rare garnet. Sagenite is locally present in biotite.

granodiorite-porphyry and granite-porphyry correspond to the sub-alkaline field, as defined by Middlemost (1997). K_2O dominates over Na_2O in granite-porphyry, whereas Na_2O dominates over K_2O in monzodiorite- to quartz monzodiorite-porphyry and granodiorite-porphyry. Nevertheless, monzodiorite- to quartz monzodiorite-porphyry belong to the high-K calc-alkaline series, and granodiorite-porphyry belongs to the medium-K calc-alkaline series or is transitional between the medium- and high-K calc-alkaline rocks (Table 2; Fig. 5B). Monzodiorite- to quartz monzodiorite-porphyry is metaluminous, whereas granodiorite-porphyry varies from metaluminous to weakly-peraluminous and corresponds to the I-type to the peraluminous I-type granites (cf. Chappell and White, 1992; Chappell et al., 2012). All rocks have Fe_2O_3/FeO slightly above or below 0.4, which defines them as being weakly reduced-weakly oxidized; this is consistent with the presence of ilmenite, titanite and rutile and indicates transitional ilmenite- to magnetite-series intrusions (after Ishihara, 1981, 2004). Monzodiorite- to quartz monzodiorite-porphyry is depleted in Ca, whereas granodiorite-porphyry is strongly enriched in Ca; the latter plot in the "calc-alkalic" to "calcic" fields on the $Na_2O + K_2O$-CaO vs. SiO_2 diagram (Fig. 5D; Frost et al., 2001). On a Rb-(Y + Nb) discrimination diagram (Fig. 5F), the rocks plot in the post-collisional granite field (Pearce, 1996). The rocks are characterized by a smooth REE distribution, with a moderate LREE enrichment (La_N/Yb_N = 5–6) and with an absent or weak Eu minimum (Table 2). The rocks exhibit gradual W accumulation toward more differentiated rocks (Fig. 5F).

7. Hydrothermal assemblages and mineralization

The hydrothermal mineral paragenesis at Agylki can be subdivided into several stages (Fig. 6). Prograde calcic skarn replaces marble and adjacent hornfels and is overprinted by retrograde skarn. Relationships of the skarns with monzodiorite- to quartz monzodiorite-porphyry dikes were not observed. Propylitic alteration overprints prograde and retrograde skarns as well as monzodiorite- to quartz monzodiorite-porphyry dikes. No skarn and propylitic alteration minerals are observed in granodiorite-porphyry dikes, thus suggesting that these dikes are younger. Phyllic alteration overprints skarns replaced by propylitic mineral assemblages as well as all dikes including granodiorite- and granite-porphyry.

7.1. Prograde calcic skarn

Prograde calcic skarn was formed over the lenticular limestone (marble) horizon and adjacent biotite (quartz-biotite ± amphibole) hornfels, and is composed of anhydrous minerals (cf. Meinert et al., 2005), principally dominant pyroxene, minor garnet, plagioclase, calcite, and locally vesuvianite. There is a skarn zonation, with a thick inner pyroxene-calcite, pyroxene, pyroxene-garnet, and/or (rarely) pyroxene-vesuvianite zone developed after marble; it is rimmed by thin pyroxene-plagioclase zone replacing hornfels at both the upper and lower contacts of the marble unit. This zonation can be multiplied several times in local intervals where thin hornfels layers are present within the marble unit (Fig. 7A). Marble remnants are locally present in the pyroxene and pyroxene-garnet skarn. The skarn is fine-grained (< 0.5–2 mm); light-green to green pyroxene has low to elevated hedenbergite content (6–12 mol.% to 24 vol% hedenbergite; Table 3), respectively, and garnet is light-brown to pale-brown isotropic grossular-rich (21–26 mol.% andradite; Table 3). The low and variable hedenbergite content (Table 3), together with the presence of vesuvianite adjacent to marble, may suggest that a minor amount of magnesian skarn could be present and then replaced in the course of prograde calcic skarn development.

7.2. Retrograde skarn

Retrograde skarn is defined as an assemblage containing both anhydrous minerals of the calc-silicate skarn paragenesis (e.g., pyroxene, garnet, plagioclase, etc.) and coexisting hydrous minerals (e.g.,

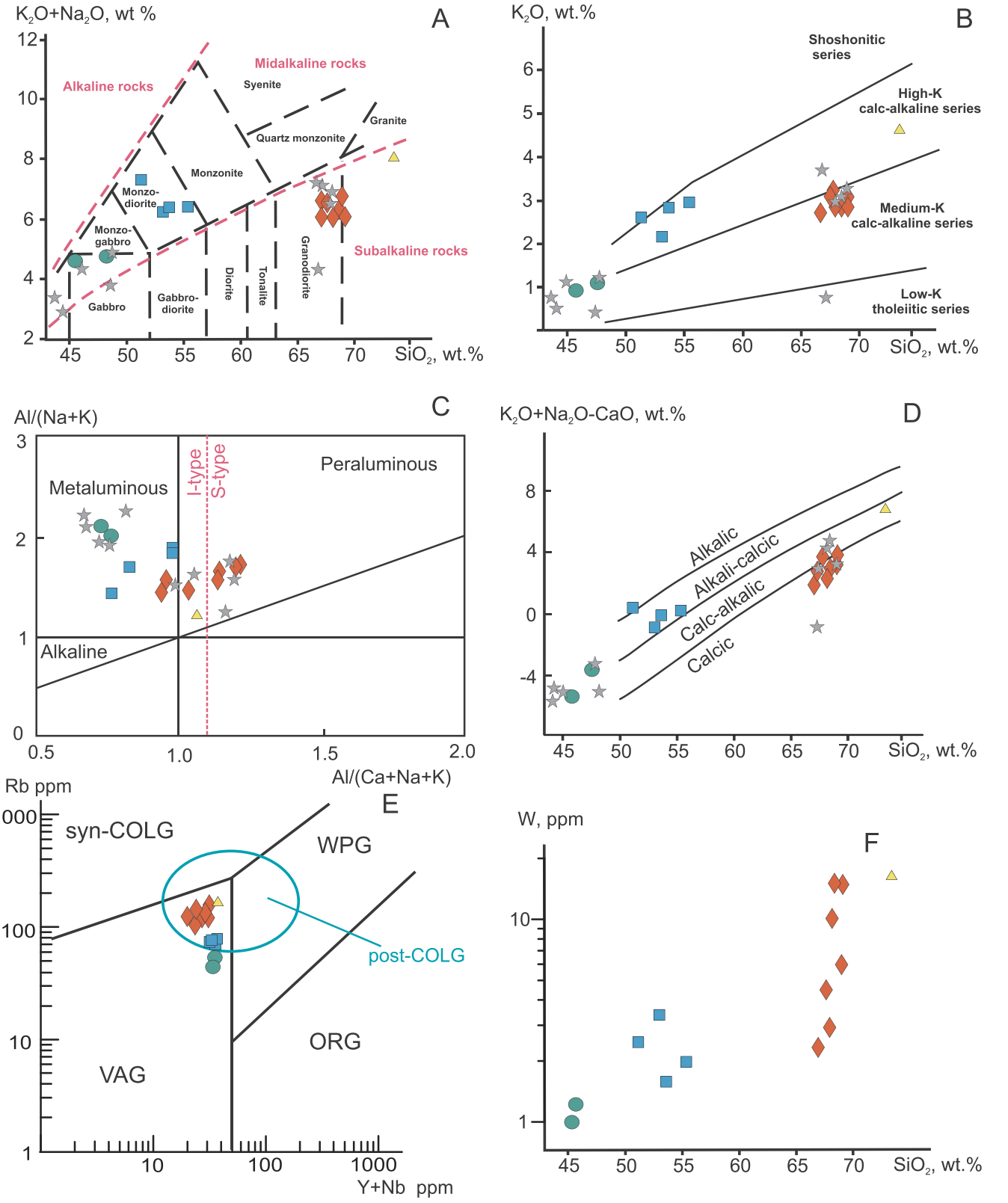

(caption on next page)

Fig. 5. Plots illustrating the chemistry of igneous rocks from the Agylki deposit. (A) SiO_2 vs. (K_2O + Na_2O) diagram for chemical compositions of plutonic rocks (after Middlemost, 1997). (B) SiO_2 vs. K_2O diagram (after Peccerillo and Taylor, 1976; Le Maitre et al., 1989). (C) Al/(Na + K) vs. Al/(Ca + Na + K) diagram defining the alkaline, metaluminous and peraluminous igneous rocks (after Maniar and Piccoli, 1989; Chappell and White, 1992). (D) (K_2O + Na_2O-CaO) vs. SiO_2 diagram defining the alkalic, alkali-calcic, calc-alkalic and calcic igneous rocks (after Frost at al., 2001). (E) Rb vs. (Y + Nb) diagram showing compositional fields of granitic rocks formed in *syn*-collisional (*syn*-COLG), post-collisional (post-COLG), volcanic arc (VAG), within-plate (WPG), and oceanic ridge (ORG) tectonic environments (after Pearce, 1996). (F) W-SiO_2 diagram showing distribution of tungsten in the igneous rocks. The individual rock compositions are from Table 2. Historical rock compositions are from Flerov et al. (1974) and Gvozdev (2010).

Table 2
Chemical composition of igneous rocks from the Agylki deposit (wt.%, ppm).

	Lamprophyre		Monzodiorite- to quartz monzodiorite-porphyry				Granodiorite-porphyry							Granite-porphyry
	1	2	3	4	5	6	7	8	9	10	11	12	13	14
wt.%														
SiO_2	45.22	47.61	51.16	53.01	53.64	55.41	66.97	67.38	67.75	68.10	68.35	68.77	69.12	73.26
TiO_2	1.37	1.15	0.81	0.71	1.28	0.89	0.47	0.46	0.45	0.45	0.44	0.42	0.42	0.24
Al_2O_3	14.81	15.97	15.32	15.53	17.86	17.44	14.12	14.21	14.56	15.28	15.63	15.40	15.21	14.90
Fe_2O_3	1.44	1.86	3.28	3.12	2.40	2.52	3.16	1.86	1.12	1.10	1.02	1.13	0.96	0.86
FeO	7.50	6.52	5.39	5.32	4.75	4.13	3.32	2.93	3.20	2.98	2.85	3.17	3.01	1.19
MnO	0.28	0.37	0.17	0.15	0.35	0.29	0.02	0.04	0.02	0.02	0.03	0.02	0.02	0.02
MgO	11.92	9.21	6.35	5.80	5.71	5.02	1.10	1.02	1.04	1.01	1.05	1.00	0.96	0.49
CaO	10.12	9.42	6.97	7.16	6.54	6.24	4.25	3.79	3.06	3.01	2.83	2.76	2.74	1.29
Na_2O	3.42	3.20	4.72	4.12	3.58	3.45	3.31	3.56	3.51	3.35	3.40	3.28	3.50	3.49
K_2O	1.13	1.21	2.60	2.16	2.83	2.95	2.77	3.11	3.21	2.89	2.84	2.79	3.02	4.64
P_2O_5	0.72	0.67	0.23	0.20	0.32	0.29	0.20	0.18	0.15	0.15	0.14	0.14	0.13	0.06
LOI	1.51	2.62	2.19	1.98	0.55	1.10	0.70	1.07	1.24	1.02	0.95	1.24	0.65	0.41
Total	99.34	99.81	99.19	99.26	99.81	99.73	100.39	99.61	99.31	99.36	99.53	100.12	99.68	100.85
ppm														
Ba	743	812	631	617	670	638	483	456	431	449	453	421	410	318
Sr	635	612	516	542	405	428	341	364	312	349	390	328	310	122
Co	43	51	23	20	39	44	7.0	7.9	8.1	7.8	10	8.1	7.4	3.1
Ni	72	84	56	49	70	68	21	28	22	24	25	23	20	14
V	243	203	140	121	129	132	94	88	90	74	61	67	70	15
Cr	78	82	39	23	43	40	4.9	7.2	6.1	4.0	4.2	5.6	4.0	2.2
Li	32	21	40	32	34	35	32	37	34	45	39	40	42	31
Rb	44	56	70	72	73	78	123	142	144	112	140	132	143	154
Be	1.2	1.5	2.1	2.0	1.9	2.3	2.2	3.2	2.8	4.3	3.0	3.2	4.1	3.8
Zr	76	71	102	91	119	115	161	143	155	142	148	140	138	121
Nb	4.5	5.2	8.0	8.4	8.5	8.9	9	11	12	10	9	12	13	15
Y	29	31	26	27	23	28	11	13	15	12	16	18	18	21
Sn	2.3	2.1	4.1	4.0	3.9	4.1	5.8	7.2	4.8	6.1	7.8	8.1	7.3	8.2
Mo	1.1	1.3	2.3	2.4	2.2	2.6	2.2	1.8	3.2	3.4	4.3	5.0	4.6	5.0
W	1.0	1.2	2.5	3.4	1.6	2.0	2.4	4.5	2.9	10.1	15.1	6.2	14.8	16.5
Cs	3.1	2.3	5.5	4.5	4.9	5.0	5.4	6.2	4.3	7.4	5.0	4.8	6.8	5.4
Hf	2.1	2.2	3.1	3.0	3.4	3.2	7.9	6.2	5.4	6.2	6.6	6.1	4.8	3.9
Ta	0.72	0.78	0.84	0.90	0.92	1.0	1.2	1.4	1.5	1.3	1.1	1.5	1.3	1.7
Th	9.2	11.4	12.1	10.8	11.2	10.0	10.4	11.3	10.6	12.1	11.0	11.3	10.5	10.4
U	2.4	2.7	4.3	4.1	3.5	3.0	2.3	2.6	2.4	3.7	4.0	4.6	3.8	3.5
Cu	15	20	54	39	32	40	34	38	43	21	44	120	30	44
Zn	25	38	58	43	34	47	49	62	38	30	45	69	65	39
Pb	18	24	31	27	26	30	36	48	27	21	35	47	42	29
La	71	66	49	61	39	43	32	37	34	39	29	41	35	24
Ce	123	118	87	92	62	71	57	72	54	70	41	68	62	40
Pr	15	14	6.9	8.0	8.2	7.1	2.4	3.2	3.1	4.4	2.9	3.2	4.0	3.4
Nd	52	57	36	39	29	31	35	29	35	31	32	38	31	29
Sm	10	13	8.1	7.2	6.5	7.2	5.4	5.1	5.6	6.2	6.5	6.4	5.9	6.7
Eu	2.7	2.4	1.2	1.3	1.3	1.2	1.1	1.1	1.2	1.0	1.0	0.9	0.9	0.7
Gd	7.6	8.1	3.3	3.2	3.4	3.5	4.2	4.1	4.4	4.0	4.5	4.3	4.6	4.0
Tb	1.1	1.2	0.82	0.89	0.83	0.80	0.63	0.66	0.71	0.68	0.66	0.74	0.67	0.88
Dy	6.8	7.2	3.6	4.0	3.8	4.0	4.2	4.4	4.1	4.0	3.8	4.5	4.8	4.3
Ho	1.4	1.5	0.67	0.72	0.67	0.75	0.79	0.84	0.92	0.80	0.74	0.83	0.88	0.81
Er	5.2	4.3	3.1	3.4	3.2	3.5	2.9	2.2	2.8	2.5	2.5	2.6	2.3	2.2
Tm	0.58	0.61	0.46	0.45	0.50	0.49	0.36	0.38	0.37	0.40	0.44	0.43	0.45	0.38
Yb	3.2	3.6	2.2	2.4	2.4	2.3	1.7	1.8	2.0	1.8	2.2	2.3	2.0	1.7
Lu	0.61	0.52	0.44	0.41	0.40	0.42	0.33	0.30	0.34	0.26	0.41	0.35	0.36	0.30

amphibole, epidote) that replace prograde (typically anhydrous) skarn. This assemblage is most developed in the prograde pyroxene skarn and occurs as pervasive to patchy replacement and/or re-crystallization of fine-grained prograde skarn pyroxene into larger (up to 2 cm long) euhedral crystals (Fig. 8A). Minor but ubiquitous amphibole (ferroactinolite to actinolite; Table 3) associated with quartz emphasizes the retrograde character of this skarn. Quartz is consistently present in retrograde skarn, initially in the interstitions of prograde skarn pyroxene crystals (corroding pyroxene) and then occupying more volume, as the process develops, with its final dominance and only minor typically euhedral re-crystallized pyroxene crystals (Fig. 8B). Pyrrhotite and trace chalcopyrite closely follow the development of quartz and re-crystallization of pyroxene, and occur as intergranular disseminations corroding prograde and locally retrograde skarn pyroxene (Fig. 8C) and

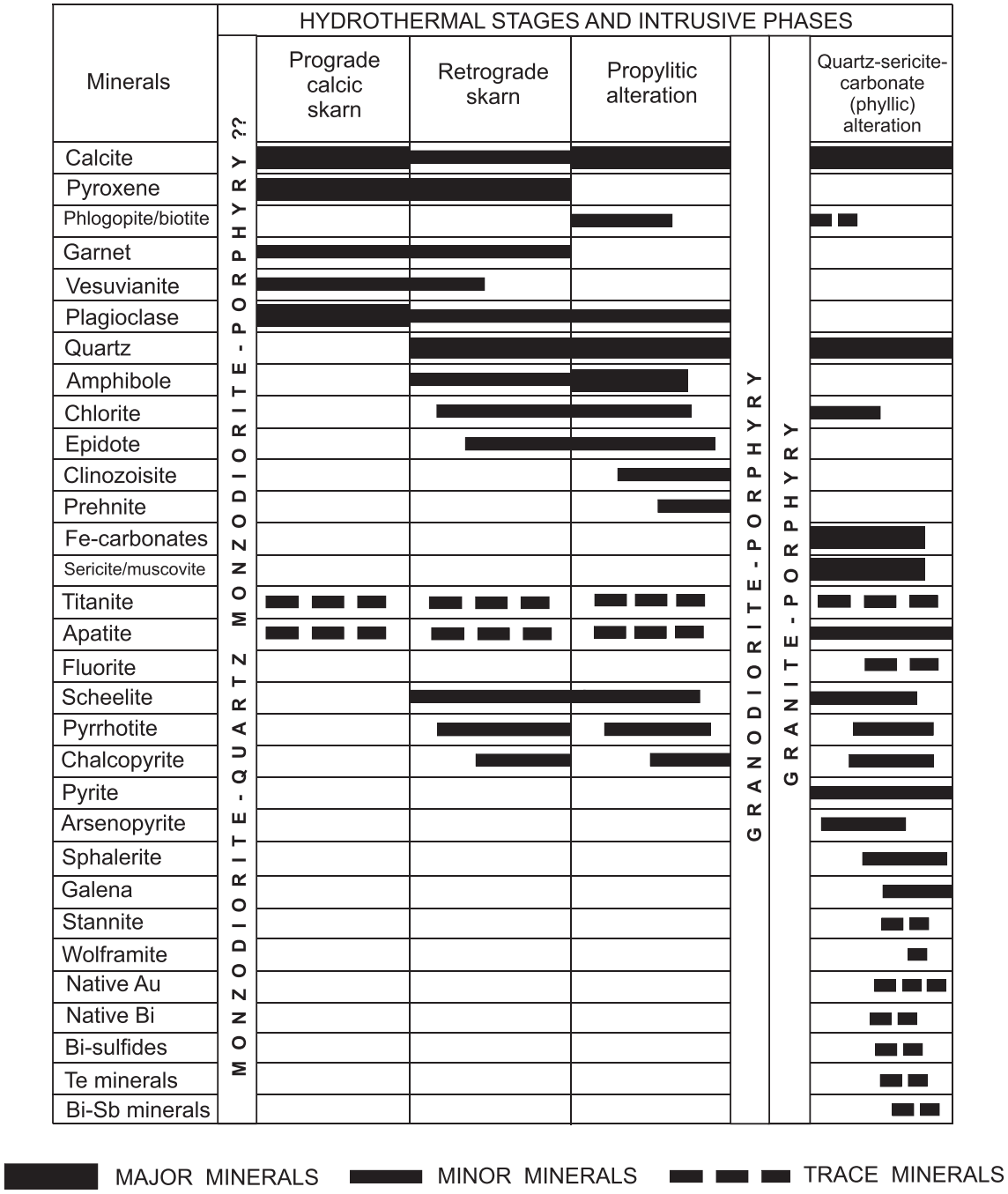

Fig. 6. Sequence of hydrothermal alteration assemblages and intrusive phases at the Agylki deposit.

then forming larger aggregates. Retrograde skarn pyroxene is dark-green and most enriched in FeO and MnO (71–81 mol.% hedenbergite and up to 11 mol.% johannsenite). Retrograde skarn garnet replaces the prograde skarn garnet, typically as outer rims and also as a granular aggregate; it is brownish-red to red (Fig. 7B), subcalcic (cf. Newberry, 1983), slightly less andraditic (11–26 mol.% andradite), and contains 12–31 mol.% spessartine + almandine (Fig. 7B; Table 3). Scheelite forms fine-grained (0.1–0.5 mm) disseminations. It has yellowish-white luminescence in ultraviolet light and slightly elevated (~0.3–0.4 wt%) Mo content. The retrograde skarn typically contains < 0.5 wt% WO_3.

7.3. Propylitic alteration

Propylitic (hydrosilicate) alteration has intense development and overprints prograde and retrograde skarns. It includes pyroxene- and garnet-free quartz-amphibole, locally oligoclase-amphibole-quartz, amphibole-chlorite-quartz, and quartz-epidote-clinozoisite-prehnite assemblages (Fig. 7C-E). The quartz-phlogopite ± amphibole ± plagioclase (oligoclase-albite) assemblage developed in biotite hornfels adjacent to the altered skarn as well as in dikes of monzodiorite- and quartz-monzodiorite-porphyry can also be assigned to propylitic alteration. Amphibole is represented by a low-Fe variety (actinolite to tremolite; Table 3) as compared to the retrograde skarn amphibole. Epidote, clinozoisite and prehnite are ubiquitous and are closely associated with pyrrhotite and particularly chalcopyrite. Chlorite is represented by clinochlore (penninite), locally by ripidolite and other varieties (Naiborodin, 1959). These assemblages replacing pyroxene skarn(s) typically contain pyrrhotite that tends to be abundant

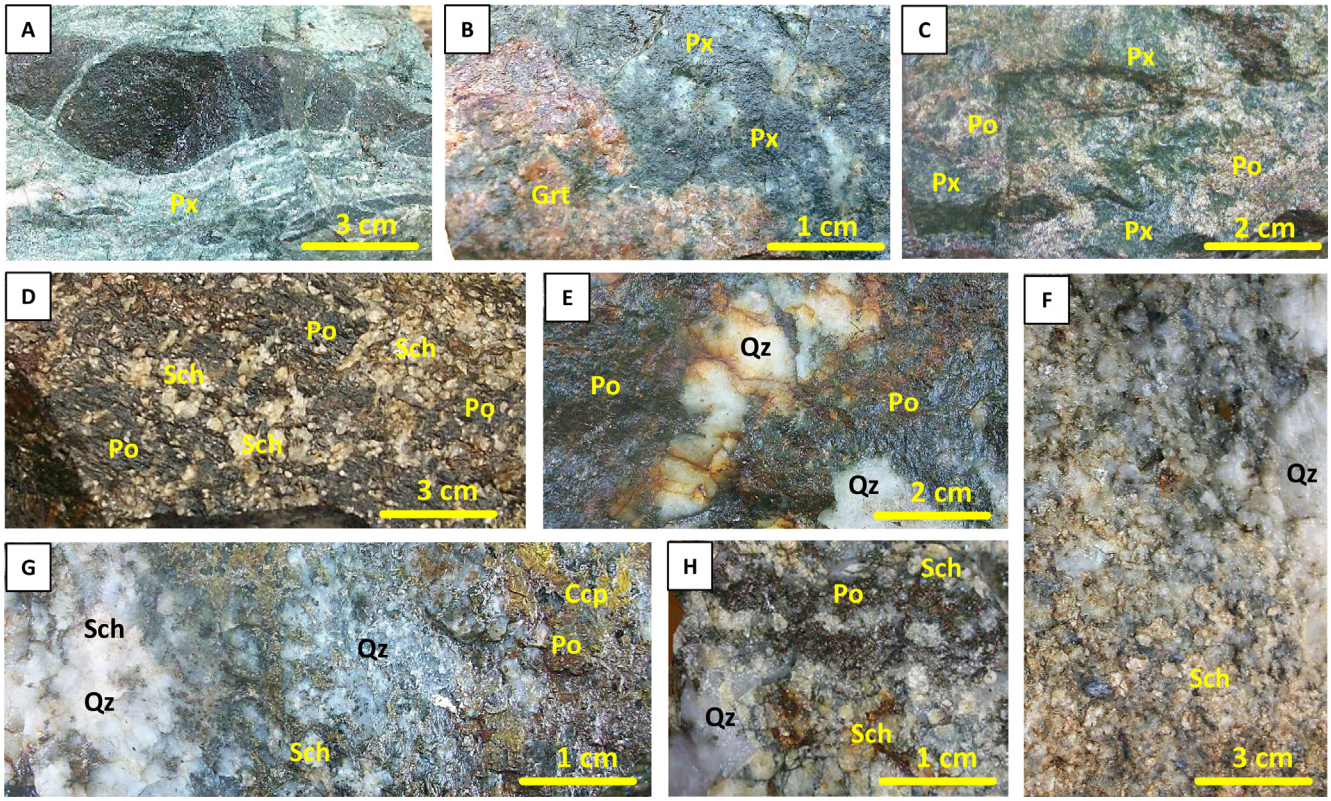

Fig. 7. Photographs showing some varieties of hydrothermal alteration at the Agylki deposit. A. Remnant of biotite hornfels in prograde pyroxene skarn. B. Retrograde skarn with subcalcic garnet (red garnet, rich in almandine + spessartine), pyroxene and quartz. C. Retrograde pyroxene-quartz skarn is replaced by propylitic pyrrhotite-amphibole-quartz assemblage. D. Propylitic assemblage with massive pyrrhotite, quartz, amphibole and abundant scheelite. E. Pyrrhotite-quartz aggregate in zone of propylitic alteration replacing pyroxene skarn. F. Coarse-grained quartz-sericite (phyllic alteration) aggregate with abundant scheelite replacing granodiorite-porphyry dike. G. Quartz-sericite-carbonate (carbonate-phyllic alteration) assemblage with scheelite, pyrrhotite and chalcopyrite replacing skarn. H. Abundant scheelite and minor sulfide minerals in a zone of quartz-sericite-carbonate (phyllic, or carbonate-phyllic) alteration. Abbreviations: Px – pyroxene, Grt – garnet, Amp – amphibole, Qz – quartz, Sch – scheelite, Ccp – chalcopyrite, Po - pyrrhotite.

(> 50 vol%) and forms massive to banded accumulations replacing pyroxene and other skarn minerals, with the development of pyrrhotite-amphibole, pyrrhotite-quartz and pyrrhotite-only aggregates (Fig. 7C-E, 8D-E). Thin layers of biotite hornfels occurring within the carbonate unit are almost entirely replaced by pyrrhotite, with minor amphibole, chlorite and quartz. Pyrrhotite is the most abundant sulfide mineral locally forming massive aggregates; it is accompanied by subordinated chalcopyrite (Fig. 9A). Scheelite is ubiquitous, particularly in association with amphibole, calcite and pyrrhotite, where small to large (1–2 mm to 0.5–1 cm) short prismatic or bipyramidal crystals and their aggregates are present (Fig. 7D, 8D-E). It has a white luminescence in ultraviolet light and a low Mo content (0.1–0.2 wt% Mo). Retrograde skarn overprinted by propylitic alteration typically contains 0.5–1 wt% WO_3.

7.4. Quartz-sericite-carbonate (phyllic to carbonate-phyllic) alteration with scheelite and sulfides

This alteration is most distinctly associated with granodiorite- and granite-porphyry dikes that crosscut the skarn zone (Figs. 3, 4); it occurs in narrow transverse zones in the form of dense stockworks (up to 2 m wide) and intervals of pervasive replacement enriched in quartz and sericite (Fig. 7F-H, 8F-H). The mineral assemblage contains dominant quartz, muscovite (sericite), minor carbonates (siderite, ankerite, calcite; up to 20 vol%), albite and chlorite (up to 10 vol% each), rare biotite, and trace colorless to light-green fluorite. Apatite is locally abundant, particularly in association with scheelite, where it forms aggregates of coarse crystals (up to 1 cm across; Fig. 8G). Quartz dominates in the central parts of phyllic alteration zones, is locally coarse-grained, with or without typically coarse-grained muscovite (sericite), whereas the intermediate parts include medium- to fine-grained quartz, muscovite (sericite), locally carbonate, albite, and the outer parts are composed of fine-grained quartz-sericite-carbonate ± chlorite aggregate. Biotite is locally present in the outer parts of phyllic alteration zones intersecting biotite hornfels. Scheelite is ubiquitous and is represented by low-Mo (typically ~0.02–0.05 wt% Mo) variety exhibiting blue luminescence in ultraviolet light. It forms typically dipyramidal crystals, is locally coarse-grained (up to 2 cm across), with correspondingly high (in excess of 3 wt%) WO_3 grades in some intervals. Overall sulfide content in zones of phyllic alteration is much lower than that in zones of pyrrhotite-rich propylitic alteration; as a result, phyllic alteration overprint causes decreasing sulfide content in altered skarns. However, zones of phyllic alteration contain a much greater variety of sulfide and sulfosalt species.

Arsenopyrite is an early mineral of this stage; it locally forms monomineralic aggregates up to 1.5 m across, typically cataclased, and is common in other locations as fine-grained dissemination (up to 10 vol%; Fig. 8F, 9B). Chalcopyrite (occasionally with minor sphalerite and/or stannite emulsion) and pyrrhotite represent new (late) generation(s) of these minerals and post-date arsenopyrite in phyllic alteration assemblages; their content typically ranges between 5 and 10 vol%. Native bismuth is closely associated with scheelite and chalcopyrite (Fig. 9C-D). Trace bismuthinite, tetrahedrite and tetradymite postdate chalcopyrite and native bismuth. Brown to dark-brown sphalerite postdates massive chalcopyrite; it is locally accompanied by stannite, native bismuth and/or bismuthinite (Fig. 9E-F). Galena occurs sporadically and post-dates sphalerite. Sphalerite contains 3.55–7.35 wt% Fe and up to 1.4 wt% Cd; galena contains 0.4–1.4 wt% Ag and 2.0–4.35 wt% Bi

Table 3
Representative microprobe analyses of pyroxene, garnet and amphibole from the Agylki deposit, wt.%, mol.%

Mineral	Pyroxene				Garnet					Amphibole			
Assemblage	Prograde skarn			Retrograde skarn		Prograde skarn			Retrograde skarn			Propylitic alteration	
	1	2	3	4	5	6	7	8	9	10	11	12	13	14	15	16	17
SiO_2, wt.%	53.44	55.12	54.62	52.18	52.39	53.10	51.44	37.01	37.54	37.12	37.23	37.50	38.01	51.02	51.96	53.14	54.41
TiO_2, wt.%	0.02	0.00	0.00	0.00	0.00	0.00	0.00	0.15	0.23	0.10	0.32	0.20	0.11	0.02	0.04	0.00	0.00
Al_2O_3, wt.%	0.78	0.93	1.12	0.64	0.43	0.21	0.10	18.32	18.01	17.93	15.52	17.18	18.15	3.72	3.80	4.10	4.04
FeO, wt.%	4.59	3.18	2.43	8.16	16.36	18.30	21.03	9.31	10.12	11.41	12.89	11.01	11.84	27.01	18.04	12.01	4.60
MnO, wt.%	0.43	0.35	0.22	0.54	2.18	2.01	2.15	0.21	0.32	0.05	2.39	6.32	7.10	1.08	1.41	1.24	1.32
MgO, wt.%	17.40	15.31	18.19	14.41	2.40	3.04	1.48	0.10	0.21	0.05	0.61	1.01	1.14	3.70	10.43	16.30	22.01
CaO, wt.%	23.18	24.15	23.01	23.50	25.81	23.01	23.28	33.14	32.61	33.18	29.65	26.10	23.18	11.28	11.50	11.46	11.21
Na_2O, wt.%														0.30	0.31	0.24	0.32
K_2O, wt.%														0.26	0.30	0.34	0.26
Total, wt.%	99.84	99.04	99.59	99.43	99.57	99.67	99.48	98.24	99.04	99.84	98.61	99.32	99.53	98.39	97.79	98.83	98.17
	Di 86	Di 89	Di 92	Di 75	Di 18	Di 20	Di 10	Alm 3	Alm 6	Alm 4	Alm 7	Alm 8	Alm 15				
	Hd 12	Hd 10	Hd 6	Hd 24	Hd 71	Hd 71	Hd 81	Adr 22	Adr 21	Adr 26	Adr 26	Adr 18	Adr 11				
	Jo 2	Jo 1	Jo 2	Jo 1	Jo 11	Jo 9	Jo 9	Grs 74	Grs 71	Grs 69	Grs 59	Grs 56	Grs 54				
								Prp < 0.5	Prp 1	Prp < 0.5	Prp 2	Prp 4	Prp 4				
								Sps < 0.5	Sps 1	Sps < 0.5	Sps 5	Sps 14	Sps 16				

Di = diopside, Hd = hedenbergite, Jo = johannsenite, Alm = almandine, Adr = andradite, Grs = grossular, Prp = pyrope, Sps = spessartine.

(Gvozdev, 2002). Trace wolframite and stibnite are locally present (Naiborodin, 1959; Dorofeev, 1961). Native gold is represented by several generations; an early generation (fineness 920–850‰) is associated with native Bi and occurs as microinclusions in chalcopyrite and pyrrhotite (Fig. 9G). Late generation(s) of native Au and electrum (fineness from 800–700‰ to 600–300‰) are associated with bismuthinite (Fig. 9H), jamesonite and/or tetradymite (Flerov et al., 1974), and other Bi-Te and/or Au-Te minerals. Gvozdev (2002) reported an early native bismuth-bismuthinite and a late galena-sulfobismuthite assemblage; the latter is more widespread and comprises Pb-Sb-Bi sulfosalts and Te minerals (Bi-jamesonite, Sb-kobellite, Sb-bismuthinite, hessite, bournonite, cozalite, zhozeite-B, hedleyite, etc.) as well as a later generation of native gold.

8. Fluid inclusion analysis

8.1. Fluid inclusions in prograde and retrograde skarn minerals

No fluid inclusions confidently regarded as primary ones and without post-entrapment modifications (cf. Roedder, 1984) have been identified in prograde skarn minerals. Consistently, the study involved fluid inclusions in retrograde skarn minerals.

Primary type 1 fluid inclusions were observed in pyroxene, quartz, and scheelite from the retrograde skarn, typically as isolated individuals (Fig. 10A-E; Table 4). They contain 1–3 anisotropic colorless (to semi-transparent white) solid phases, and a small (10–20 vol%) gas bubble. No halite or sylvite was identified. On freezing/warming, type 1 fluid inclusions exhibit eutectic melting temperatures at −34 °C to −31 °C (indicating dominant NaCl but with an admixture of $MgCl_2$; Crawford, 1981), and final ice melting temperatures of −13.5 to −10.1 °C. In the pure NaCl-H_2O system, this corresponds to a salinity of 14.0–17.3 wt% NaCl (Table 4; Bodnar and Vityk, 1994). On heating, the gas bubble disappears at 320–340 °C (Table 4).

8.2. Fluid inclusions in propylitic alteration minerals

Primary and pseudosecondary fluid inclusions in quartz and scheelite from the propylitic alteration assemblage occur mostly in clusters and are represented by liquid-gaseous type 2 inclusions containing a medium- to small-sized (30–40 vol% to 15–20 vol%) gas bubble (Fig. 10F-I; Table 4). No halite or sylvite was identified. On freezing/warming, type 2 fluid inclusions exhibit eutectic melting temperatures below −50 °C (up to −55 °C) indicating the presence of $CaCl_2$ (Crawford, 1981), and final ice melting temperatures of −9.8 to −5.7 °C. In the pure NaCl-H_2O system, this corresponds to salinity of 13.7–8.8 wt% NaCl (Table 4; Bodnar and Vityk, 1994). On heating, the gas bubble in type 2 fluid inclusions with variable gas/liquid ratio disappears at a broad range of temperatures from 220 °C to 290 °C (Table 4).

8.3. Fluid inclusions in minerals from quartz-sericite-carbonate (phyllic to carbonate-phyllic) alteration

Primary and pseudosecondary fluid inclusions found in quartz and scheelite from these alteration zones are represented by two (older and younger) fluid inclusion assemblages occurring in clusters and short trails in minerals. The older assemblage is represented by coexisting essentially gaseous (80–100 vol% gas) type 3A and liquid-gaseous (30–40 vol% gas) type 3B inclusions, both containing variable amounts of carbonic species (Fig. 10J-L). On warming after freezing, CO_2 melting in type 3A inclusions occurs at −64.0 + 0.3 °C indicating significant methane contents. Further warming reveals the temperatures of carbonic phase homogenization to liquid at −15 to −10 °C (Table 4). This allows estimation of CH_4 mole fraction at 0.4 (40 mol.%) and molar volume of carbonic phase of 70–75 cm^3/mole (Thiery et al., 1994). In type 3B inclusions, on warming after freezing, a phase of CO_2

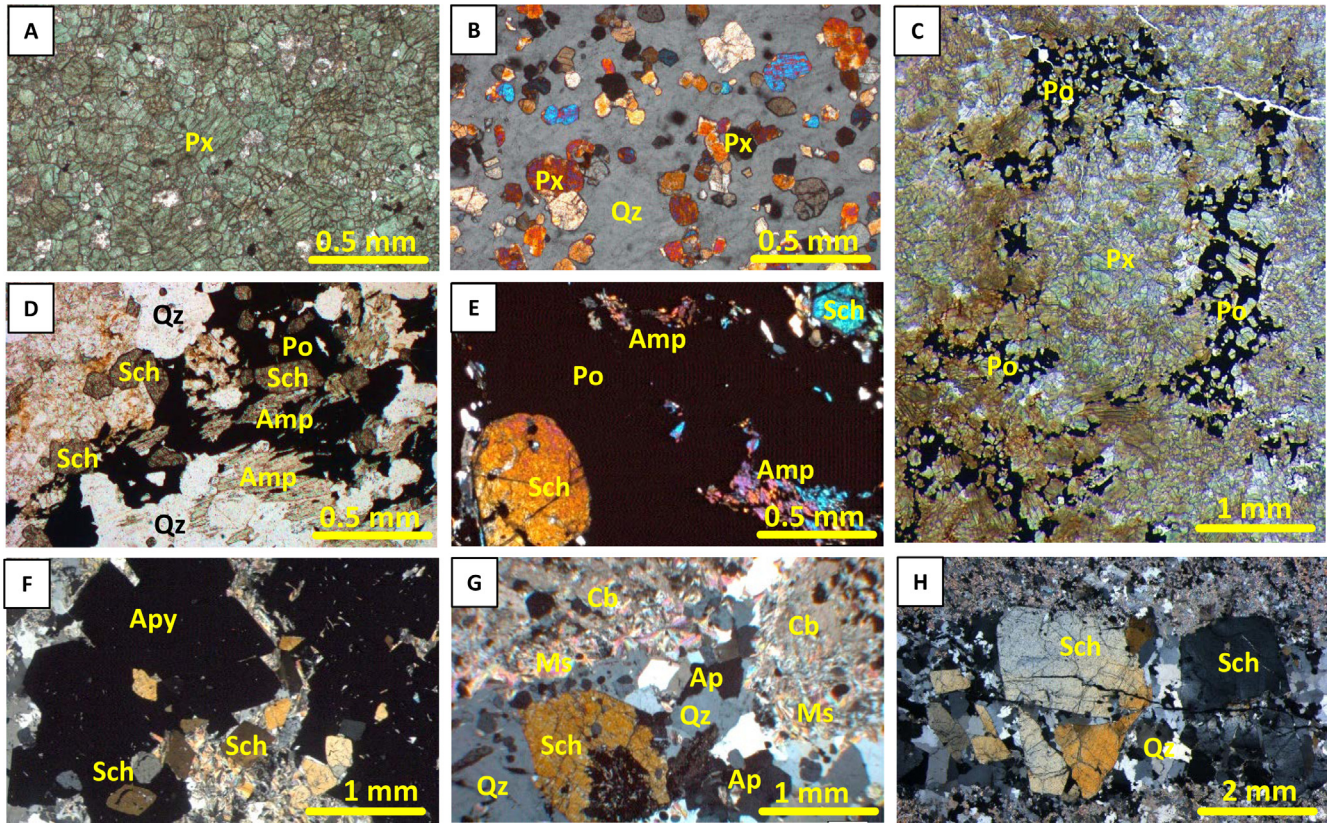

Fig. 8. Photomicrographs showing relationships of minerals from the Agylki deposit. A. Fine-grained pyroxene in prograde calcic skarn weakly replaced by coarser-grained retrograde skarn minerals (thin section). B. Quartz-pyroxene retrograde skarn; re-crystallized pyroxene tends to become euhedral (thin section, nicols crossed). C. Fine-grained pyroxene of prograde calcic skarn is replaced by coarser-grained retrograde skarn pyroxene-quartz-pyrrhotite assemblage (thin section). D. Retrograde pyroxene skarn is replaced by propylitic quartz-amphibole-pyrrhotite assemblage with scheelite (thin section). E. Massive pyrrhotite with amphibole and scheelite (propylitic alteration) (thin section, nicols crossed). F. Scheelite and arsenopyrite in a zone of phyllic (to carbonate-phyllic) alteration (thin section, nicols crossed). G. Scheelite and apatite in a zone of phyllic (to carbonate-phyllic) alteration (thin section, nicols crossed). H. Quartz-scheelite veinlet in a zone of phyllic (to carbonate-phyllic) alteration (thin section, nicols crossed). Abbreviations: Qz – quartz, Px – pyroxene, Cb – carbonate, Amp – amphibole, Ap – apatite, Ms – muscovite (sericite), Sch – scheelite, Po – pyrrhotite, Apy - arsenopyrite.

melts at −61.0 to −60.5 °C indicating also significant methane content; further warming reveals the temperatures of carbonic phase homogenization to liquid at +10 to +15 °C (Table 4). Clathrate melting in type 3B inclusions occurs at +10 to +12 °C, thus confirming a high methane content (Burruss, 1981). High methane content precluded from defining fluid salinity by clathrate melting temperature. On heating, type 3B inclusions homogenize into the liquid phase (by carbonic phase dissolution in water) at 280–320 °C (Table 4).

A younger generation of primary to secondary fluid inclusions in the phyllic alteration minerals is represented by liquid-gaseous (15–30 vol % gas) type 4 inclusions (Fig. 10M-P; Table 4). These inclusions, on freezing/warming, exhibit eutectic melting temperatures at −25 °C to −20 °C (indicating dominant NaCl; Crawford, 1981), and final ice melting temperatures of −14.0 to −10.0 °C. In the pure NaCl-H_2O system, this corresponds to a salinity of 14.0–17.8 wt% NaCl (Bodnar and Vityk, 1994). On heating, type 4 inclusions homogenize into the liquid phase at 200–250 °C (Table 4).

8.4. Temperature and pressure estimate

The petrologic data on hydrothermal alteration mineral paragenesis allow estimates of the respective temperature and pressure conditions. In particular, due to the lack of wollastonite, the temperature of the prograde skarn formation can be estimated within a lower range of 600–450 °C (Burt, 1977; Einaudi et al., 1981; Johnson and Norton, 1985; Meinert, 1992; Meinert et al., 2005). This is consistent with the stability of andradite-grossular garnet (10–40 mol.% grossular) at temperatures of 500–600 °C and pressures of 1500–2000 bars under low X_{CO2} (< 0.1) (Taylor and Liou, 1978), whereas diopside to diopside-hedenbergite pyroxene is stable at lower temperatures extending to ~450 °C (Gustafson, 1974). The retrograde skarn was formed at a thermal decline evident by expanded stability of hydrous silicates (amphibole, epidote, etc.), with andradite-grossular garnet becoming unstable at temperatures below 400 °C (Johnson and Norton, 1985). Hedenbergitic pyroxene is stable to temperatures below 400 °C (Gamble, 1982), and this corresponds to the lower temperature limit of retrograde skarn formation. Amphibole (tremolite) in low-CO_2 fluids (X_{CO2} < 0.3) and 2000 bars of total pressure is stable to ~430–390 °C (Einaudi et al., 1981); this corresponds to a transition from retrograde skarn to propylitic alteration, with chlorite stability extending further to lower temperatures (Jowett, 1991). Epidote is stable at temperatures as low as ~250 °C under pressures of 2–3 kbars, whereas prehnite stability extends further to temperatures of ~200 °C and pressures of < 2 kbars (Liou, 1993). Thus, ubiquitous epidote and prehnite indicate an evolution toward the lower temperature-lower pressure conditions during propylitic alteration at Agylki.

The gas bubble homogenization temperatures measured for type 1 fluid inclusions in minerals of the retrograde skarn (320–340 °C; Table 4) are lower than the possible temperatures of retrograde skarn formation estimated to be at the lower part of the ~450–600 °C range. Attributing this difference to the respective pressure correction, pressure can be estimated for multiphase type 1 inclusions using the data on isochores for H_2O-NaCl solution of salinities most closely corresponding to those defined in this study (i.e., about 15–20 wt% NaCl-eq.) (Fig. 11).

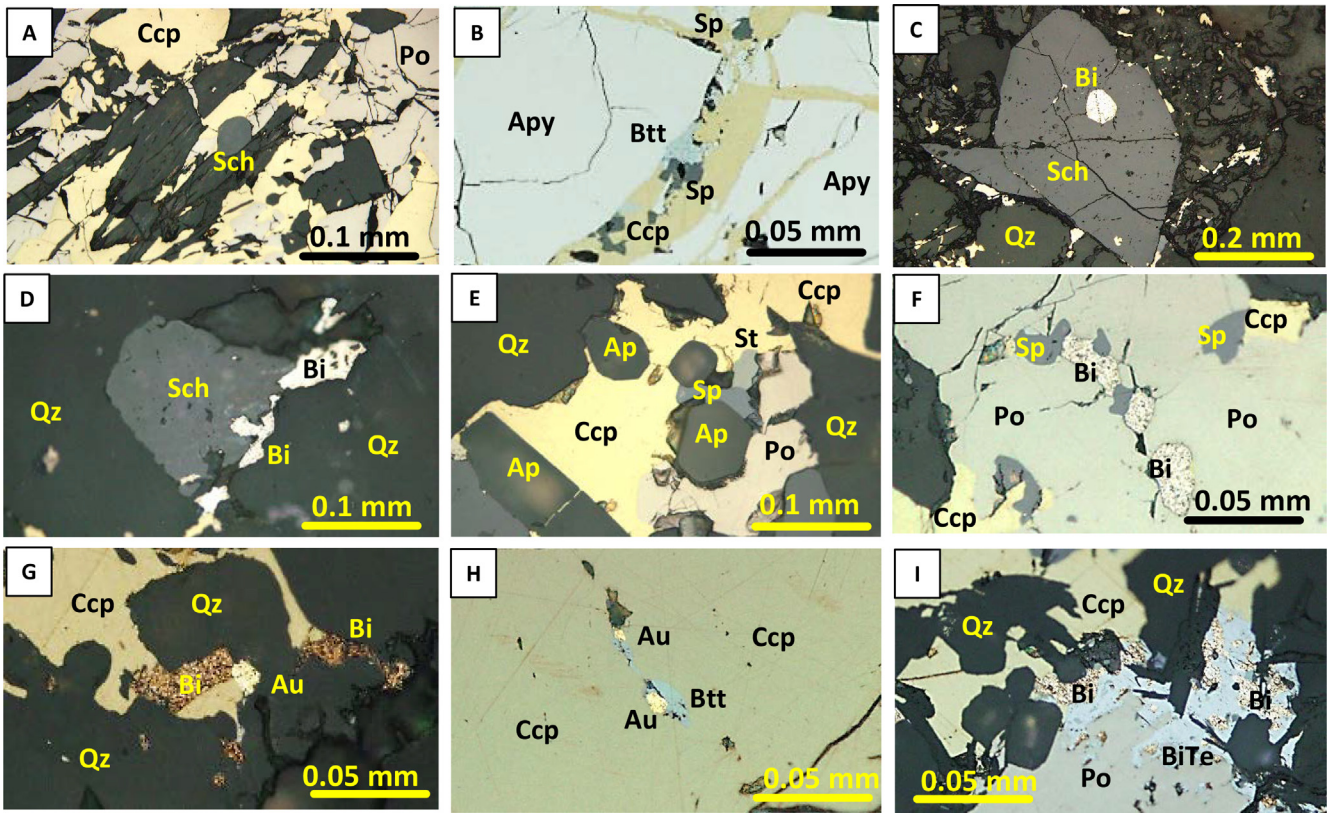

Fig. 9. Photomicrographs of polished sections showing relationships of Bi and Au minerals in propylitic and phyllic (to carbonate-phyllic) alteration assemblages at the Agylki deposit. A. Early chalcopyrite and pyrrhotite form intergrowths with amphibole in zone of propylitic alteration overprinting skarn. B. Chalcopyrite microveinlet with sphalerite and bismuthinite in brecciated arsenopyrite (phyllic alteration). C. Rounded (droplet-like) microinclusion of native bismuth in scheelite. D. Native bismuth in a microveinlet along scheelite grain boundary. E. Stannite and sphalerite with apatite, chalcopyrite and pyrrhotite. F. Sphalerite and native bismuth form microveinlet in pyrrhotite. G. Native bismuth and native gold on the edges of chalcopyrite aggregate. H. Chain of microinclusions (part of a microveinlet?) of native gold and bismuthinite in chalcopyrite. I. Native bismuth and a Bi-Te phase replacing pyrrhotite and chalcopyrite. Abbreviations: Qz – quartz, Sch – scheelite, Apy – arsenopyrite, Po – pyrrhotite, Ccp – chalcopyrite, Sp – sphalerite, St – stannite, Au – native gold, Bi – native bismuth, Btt – bismuthinite, BiTe – Bi-Te mineral.

These estimates yield a moderate pressure of 1.4 ± 0.2 kbars (Table 4), which correspond to a depth of ~5–6 km assuming lithostatic conditions (Fournier, 1999).

Similarly, the gas bubble homogenization temperatures measured for type 2 fluid inclusions in minerals of propylitic alteration (220 °C to 290 °C; Table 4) are lower than the temperatures of fluid inclusion entrapment in these mineral assemblages at Agylki. The latter can be assumed at ~350–400 °C during the early propylitic alteration at Agylki, which is consistent with the abundance of amphibole and chlorite, later evolving to ~350–300 °C, as evidenced by the presence of epidote and prehnite. Again, pressure can be estimated for type 2 inclusions using the data on isochores for H_2O-NaCl solution of salinities most closely corresponding to those defined in this study (i.e., about 10–15 wt% NaCl-eq.) and the respective temperatures of mineral deposition (i.e., true temperatures of fluid inclusions entrapment) defined by mineral paragenesis at 400–350 °C to 350–300 °C (Fig. 11). These estimates yield pressures of 1.1 to 0.8 kbar (Table 4), which correspond to a depth of ~4 km assuming lithostatic conditions (Fournier, 1999).

The presence of coexisting essentially gaseous type 3A and aqueous-gaseous type 3B inclusions in the same clusters supports their contemporaneous entrapment in the two-phase immiscibility field. If so, the trapping pressures for these fluid inclusions can be established using the trapping temperatures, the densities for type 3A fluid inclusions, and the equation of state for the CH_4-CO_2 system (Bakker, 2003). Considering the possibility of heterogeneous fluid entrapment, the measured temperatures of type 3B fluid inclusion homogenization (280–320 °C) are taken as true entrapment temperatures. The densities of carbonic phase containing CH_4 in addition to CO_2 can be determined by the diagrams from Thiery et al. (1994), using final CO_2 phase melting and carbonic phase homogenization temperatures measured. Accordingly, a density of 70–75 cm^3/mole under CH_4 mole fraction of 0.4 has been determined for type 3A inclusions; considering fluid inclusions entrapment at 280–320 °C and using the computing programs of Bakker (2003), a pressure of ~0.9 ± 0.1 kbar has been obtained.

The pressures estimated for the fluid inclusions entrapment during the phyllic alteration stage correspond to a depth of ~4 km assuming lithostatic conditions (Fournier, 1999). These estimated trapping pressures would be consistent with the porphyry features of the dikes at Agylki, thus indicating hypabissal levels. Thus, this depth of deposit formation was similar or shallower than that at many other reduced W skarn deposits (Gerstner et al., 1989; Yuvan, 2006; Guy et al., 1988; Fonteilles et al., 1989; Soloviev et al., 2017a,b; Soloviev and Kryazhev, 2017, 2018a).

9. Discussion

The Agylki W deposit is a large (> 100 Kt WO_3) and high-grade (1.27% WO_3) tungsten skarn deposit in the Verkhoyansk fold-and-thrust orogenic belt, and consistently is one of the largest W and specifically W skarn deposits in Eastern Siberia. Furthermore, it is one of the largest W skarn deposits in the Northwest Pacific. The deposit bears distinct signatures of the reduced type of W skarn deposits; thus, comparison of these deposits can contribute to establishing an integrated geological-genetic model of this type of mineral systems. The

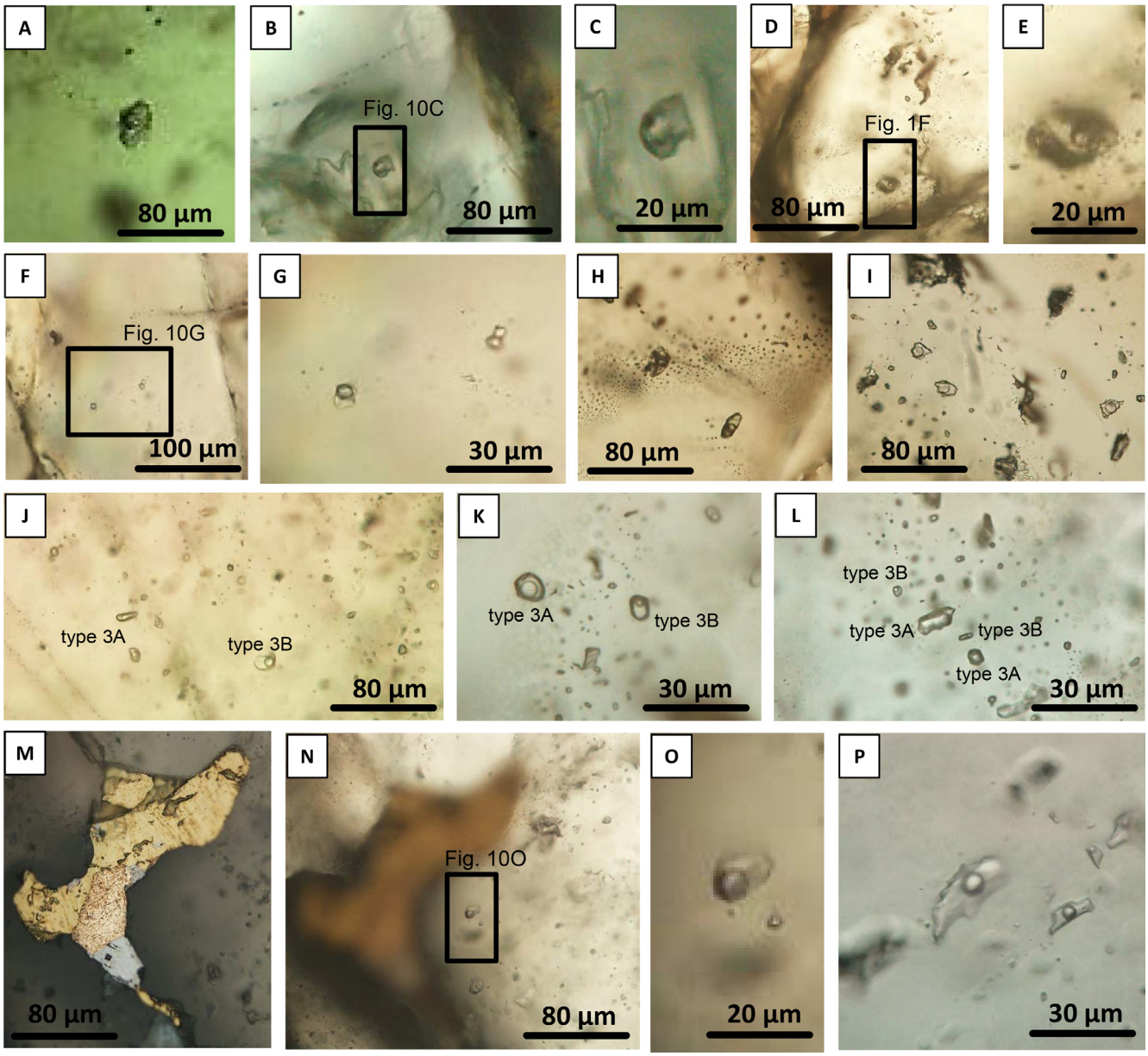

Fig. 10. Types of fluid inclusions in minerals from various hydrothermal alteration assemblages at the Agylki deposit. A-C. Multisolid type 1 fluid inclusions in pyroxene from retrograde skarn (C– larger view). D-E. Multisolid type 1 fluid inclusions in scheelite from retrograde skarn (E – larger view). F-G. Liquid-gaseous type 2 fluid inclusions in quartz from propylitic alteration assemblage (G – larger view). H-I. Liquid-gaseous type 2 fluid inclusions in scheelite from propylitic alteration assemblage. J. Coexisting gaseous-liquid type 3A and liquid-gaseous type 3B fluid inclusions in quartz from phyllic (to carbonate-phyllic) alteration assemblage. K-L. Coexisting gaseous-liquid type 3A and liquid-gaseous type 3B fluid inclusions in scheelite from phyllic (to carbonate-phyllic) alteration assemblage. M – P. Liquid-gaseous type 4 fluid inclusions in quartz from phyllic (to carbonate-phyllic) alteration assemblage (M – N – fluid inclusions near chalcopyrite-native bismuth-bismuth telluride aggregate, N – re-focused view, O – larger view).

presence of significant W mineralization in the reduced-type skarns, together with dominating reduced intrusion-related to orogenic type Au deposits in the Verkhoyansk-Kolyma orogenic system, highlights the Au-W geochemical association in the post-subduction tectonic settings (e.g., Thompson et al., 1999).

The Agylki deposit bears signatures of the reduced type of W skarn deposits, thus complementing this deposit group (type) (Sato, 1980; Einaudi et al., 1981; Kwak and White, 1982; Dick and Hodgson, 1982; Kwak, 1987; Meinert et al., 2005; Soloviev et al., 2017a,b; Soloviev and Kryazhev, 2017, 2018a). Such signatures include its association with a pluton of the transitional magnetite-ilmenite series, dominance of pyroxene skarn (with minor garnet skarn), abundance of pyrrhotite and lack of magnetite in skarns and post-skarn alteration assemblages, high hedenbergite and elevated johannsenite contents in pyroxene, together with high grossular and almandine + spessartine contents in garnet, low Mo content in scheelite and other features indicating low fO_2 conditions of the deposit formation (cf. Meinert et al., 2005). Fluid inclusion data further support a reduced environment, as methane is abundant in the fluids at Agylki, similarly to that at other reduced W skarn deposits (Bowman et al., 1985; Mathieson and Clark, 1984; Gerstner et al., 1989; Yuvan, 2006; Soloviev et al., 2017a,b; Soloviev and Kryazhev, 2017, 2018a). By its reduced W skarn signatures, Agylki differs from other W (mainly oxidized-type) deposits in the Verkhoyansk-Chukotka metallogenic province, which are situated in different terranes, are related to magnetite-series intrusions, and comprise garnet-dominant skarns with high-Mo scheelite (Goryachev et al., 2018).

Table 4
Types of fluid inclusions (FI) in minerals from various hydrothermal assemblages of the Agylki deposit.

Mineral (number of FI measured)	FI type	FI size	FI content	T_m eu., °C	T_m CO_2, °C	T_m ice, °C	T_h carb, °C	T_m clathrate, °C	Mode and temperature of final homogenization, T_h, °C	Estimated salinity, wt.% NaCl-eq.	Estimated CO_2/CH_4 ratio[b]	Estimated pressure, kbars, and T_h correction
Retrograde quartz-pyroxene-amphibole skarn with scheelite and sulfides												
Pyroxene, quartz, scheelite (18)	1	5–25 μm	Multisolid, no halite: 1–3 solids, 20–25 vol% gas	−34 to −31		−13.5 to −10.1			Gas to liquid at 320–340	14.0–17.3[a]		1.4 ± 0.2 [c] 150
Quartz-amphibole-chlorite (propylitic) alteration assemblage with scheelite and sulfides												
Quartz, scheelite (42)	2	5–30 μm	Gaseous-liquid, 30–40 to 15–20 vol% gas	−55 to −50		−9.8 to −5.7			Gas to liquid at 220–290	13.7–8.8[a]		1.1–0.8[c] 100
Quartz-sericite-carbonate (phyllic to carbonate-phyllic) alteration assemblage with scheelite and sulfides												
Quartz, scheelite (20)	3A	5–20 μm	Gaseous to gaseous-liquid; 80–100 vol% gas		−64.0 ± 0.3		−10…−15				1.5	0.9 ± 0.1[d]
Quartz, scheelite (25)	3B	5–20 μm	Liquid-gaseous; 30–40 vol% gas		−60.5..−61.0		+10…+12	+10 to + 12	Gas to liquid at 280–320		4.0	
Quartz, scheelite (22)	4	5–40 μm	Liquid-gaseous; 15–30 vol% gas	−25 to −20		−14.0 to −10.0			Gas to liquid at 200–250	14.0–17.8		

T_m eu. – eutectic temperature (first ice melting temperature), °C; T_m CO_2 – final CO_2 melting temperature, °C; T_m ice – final ice melting temperature, °C; T_h carb – carbonic phase homogenization temperature (to liquid phase), °C; T_m clathrate – final clathrate melting temperature, °C.

[a] Salinity was estimated by final ice melting temperature (Bodnar and Vityk, 1994).

[b] The ratio was estimated by final CO_2 melting and carbonic phase homogenization temperatures (Thiery et al., 1994).

[c] The trapping pressure and T_h correction was estimated by using the salinity of fluid inclusions, homogenization temperature (T_h), and the temperature of mineral formation defined by mineral paragenesis (Roedder, 1984).

[d] The pressure was estimated by using the T_h of type 3B fluid inclusions and the density of type 3A fluid inclusions trapped contemporaneously (Bakker, 2003).

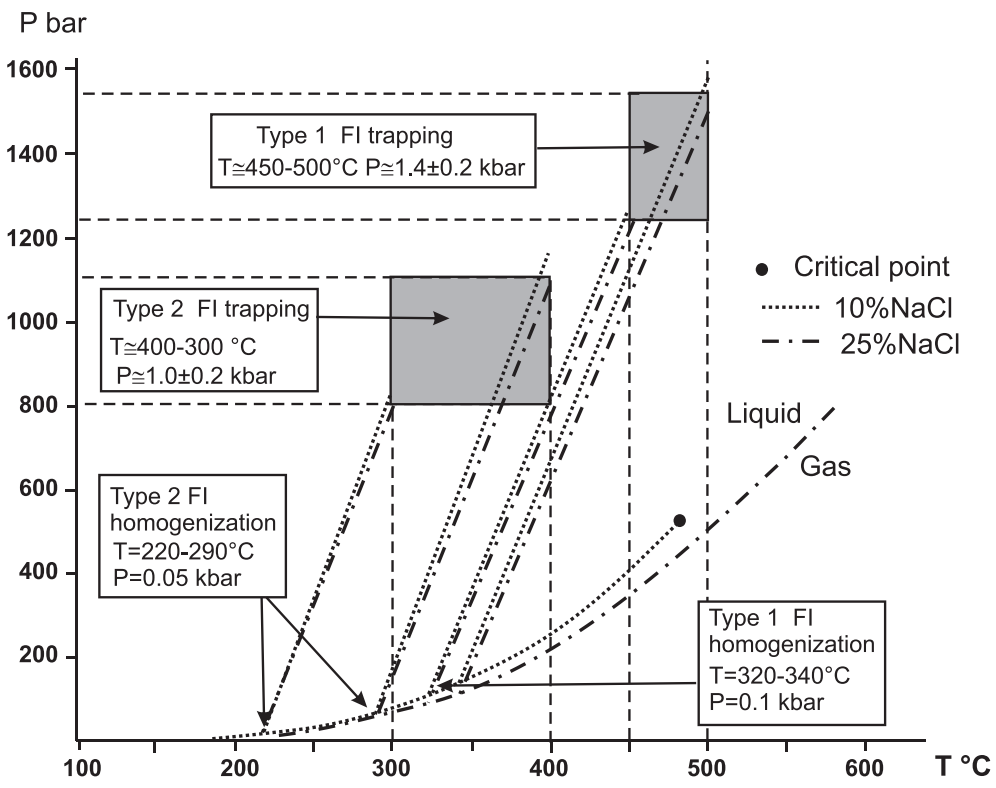

Fig. 11. Pressure estimates for the formation conditions of retrograde skarn and propylitic alteration at the Agylki deposit using the type 1 and 2 fluid inclusion (FI) homogenization temperatures (Table 4) and the temperatures estimated by mineral paragenesis. The liquid–gas curves and isochors (corresponding to various salinities, wt% NaCl) are from Roedder (1984).

9.1. Regional tectonic and metallogenic setting: global analogies

The regional tectonic setting of the Agylki deposit corresponds to an accretion-collisional terrane that was established in the outer (peripheral) zone of the Verkhoyansk-Kolyma orogenic system during the accretion and early-collisional stages, with subsequent formation of the Verkhoyansk fold-and-thrust belt in the Late Jurassic- Early Cretaceous (cf. Parfenov, 1995; Parfenov and Kuzmin, 2001; Goryachev et al., 2018). Layer et al. (2001) distinguished two stages of tectonic and magmatic activity in south-western part of the Verkhoyansk-Kolyma orogenic system, where the early subduction event along the south-western margin of the Kolyma-Omolon supperterrane, part of this system, with apparent ages of ca. 160–140 Ma, was followed by a superposed collisional event dated at 143–138 Ma. These tectonic phases are interpreted to represent subduction under and accretion to Asia followed by local extension (Layer et al., 2001). Goryachev (1999) highlighted the role of the Late Jurassic-Early Cretaceous (150–130 Ma) accretion-collisional, locally also transform-like translation, processes and corresponding formation of the Verkhoyansk fold-and-thrust belt and the activation of magmatic sources both in the granitic-metamorphic basement (including its lower parts) and overlying sedimentary sequences. This was followed by the formation of the metallogenic belts comprising dominant orogenic-type and intrusion-related Au mineralization, the latter most distinctly associated with the series of Late Jurassic-Early Cretaceous granitoid dikes (Goryachev, 1999; Volkov et al., 2010).

The model of accretion-collision to transform-like translation was suggested for many regions hosting reduced-type W skarn deposits globally and specifically in the North Pacific. In particular, in the Northwest Pacific (Sikhote-Alin orogenic system), subduction in the Triassic-Late Jurassic was accompanied by the development of the Jurassic accretionary prism, with establishing a transform plate margin and a strike-slip displacement of the early Paleozoic continental blocks, initiation of turbidite basins, and intense deformation of the Jurassic and Early Cretaceous terranes (Khanchuk et al., 2016). In the Early to early Late Cretaceous, numerous granitoid suites with mixed mantle-crustal signatures were emplaced including those accompanied by Au deposits as well as reduced W skarn deposits (Vostok-2, Lermontovskoe, Skrytoe; e.g., Soloviev et al., 2017a,b; Soloviev and Kryazhev, 2017). Asthenospheric mantle upwelling through a slab window and subcontinental lithosphere delamination represent the two possible mechanisms to explain the widespread melting of crustal rocks and emplacement of the Early to early Late Cretaceous granitoid suites exhibiting mixed crustal-mantle geochemical signatures, specifically those accompanied by reduced W skarn deposits (e.g., Jahn et al., 2015).

Similarly, in the Northeast Pacific (northern Canadian Cordillera, Selwyn Basin), voluminous Cretaceous magmatism followed subduction and accretion along the ancestral west coast of North America, when Proterozoic metasedimentary rocks and Cambrian to Devonian passive margin rocks were deformed into an outer fold-and-thrust belt with transpressional structures (e.g., Nelson and Colpron, 2007; Rasmussen et al., 2011). Khudoley (2003) has further demonstrated similarities in the tectonic evolution of passive continental margins that were developed to the east of the Siberian craton and to the west of the North American craton, respectively. Large reduced W skarn deposits (Can-Tung, MacTung) in the Selwyn Basin are associated with Cretaceous intrusions derived due to mingling of ascending mafic magmas with silicic magmas, the latter generated from the accretionary complex, producing hybrid I-S type granitoid magma (Rasmussen et al., 2011).

Consistently, reduced W skarn deposits appear to be typical for the tectonic settings in accretion-collisional, locally transform-type, outer (pericratonic) thrust-and-fold belts developed over passive continental margins, to various degree subjected to collisional granitoid magmatism with mixed mantle-crustal geochemical signatures. This differs reduced W skarn deposits from oxidized W-Mo-Cu skarn deposits formed in subduction-related settings and associated with the magnetite-series intrusions (e.g., Meinert, 1995). This also differs reduced W skarn deposits from redox-intermediate W-Mo skarn deposits formed in the post-collisional to within-plate orogenic settings that were characterized by a greater contribution from a long-term radiogenic source such as an old continental crust, rather than from accretionary type

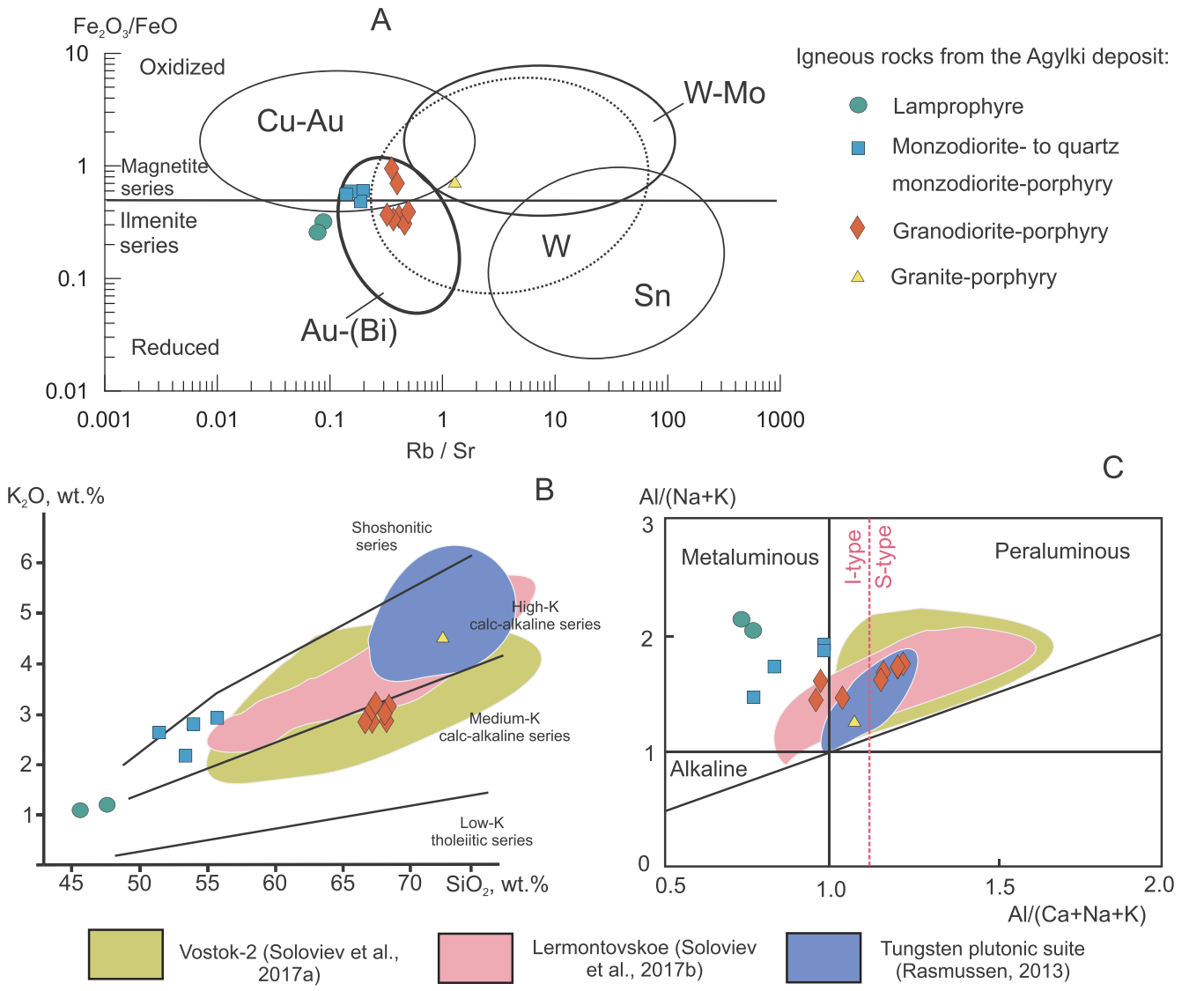

Fig. 12. A. Compositions of the igneous rock from the Agylki deposit shown on the schematic plot of degree of fractionation (Rb/Sr ratio) versus the oxidation state (Fe_2O_3/FeO) for igneous rocks associated with Cu-Au, W-Mo, Au-(Bi) and Sn mineralization (Baker et al., 2005). B-C. Comparison of compositions of the igneous rocks from the Agylki deposit with igneous rocks from some other reduced W skarn deposits (Soloviev and Kryazhev, 2018a). The individual rock compositions are from Table 2.

reservoirs, in the formation of parental granitoids, with an increasing Mo endowment in regions with thicker continental crust (e.g., Soloviev and Kryazhev, 2018, 2019).

9.2. Igneous rocks: magma sources and evolution

The parental plutonic suite at Agylki comprises ilmenite-titanite-bearing, medium- to high-K calc-alkaline, metaluminous to peraluminous I-type granitoid rocks. On the Fe_2O_3/FeO vs. Rb/Sr diagram (Fig. 12A), the rocks are plotted in the W and Au(+Bi) deposit fields. The latter is consistent with the regional association of most intense W and Au mineralization with this or a similar Late Jurassic-Early Cretaceous dike suite (Goryachev, 1999; Volkov et al., 2007). As compared to the igneous suites related to some other reduced W skarn deposits (Newberry, 1998; Newberry and Swanson, 1986; Rasmussen et al., 2011; Rasmussen, 2013; Soloviev et al., 2017a,b; Soloviev and Kryazhev, 2018a), the rocks are characterized by lower Al saturation index, with correspondingly lesser peraluminous signature, under lesser enrichment in K (Fig. 12B–C).

The Agylki igneous rocks are distinctly divided into two groups with contrasting composition, the early group of mafic (monzodiorite- to quartz monzodiorite-porphyry) composition, and the late group of silicic (granodiorite- to granite-porphyry) composition. Consistently, if the first group shows a strong metaluminous signature, moderate to strong enrichment in K, Mg, Ti and P, the second group exhibits transitional metaluminous to peraluminous compositions, with much stronger enrichment in Ca and depletion in K, Ti and P, together with an enrichment in Zr and Hf (Fig. 13). This may indicate different magma sources. Specifically, a deeper (possibly mantle-related) mafic magma source can be envisioned for the first group, whereas a dominantly crustal magma source may have produced the second group rocks. Moreover, there is a certain geochemical affinity of the monzodiorite- to quartz monzodiorite-porphyry to the older lamprophyre dikes that in expressed in the low Nb but elevated Ta, Nd, Sm contents in the both rock varieties (Fig. 13). This affinity is further preserved in the granodiorite-porphyry, thus suggesting that the granitoid magma could be induced at crustal levels under an influence of much deeper, mantle-derived magma. Notably Nikonov (2004) suggested that lamprophyre dikes may represent precursors to more intense granitoid magmatism accompanied by Au deposits in the Verkhoyansk-Kolyma orogenic

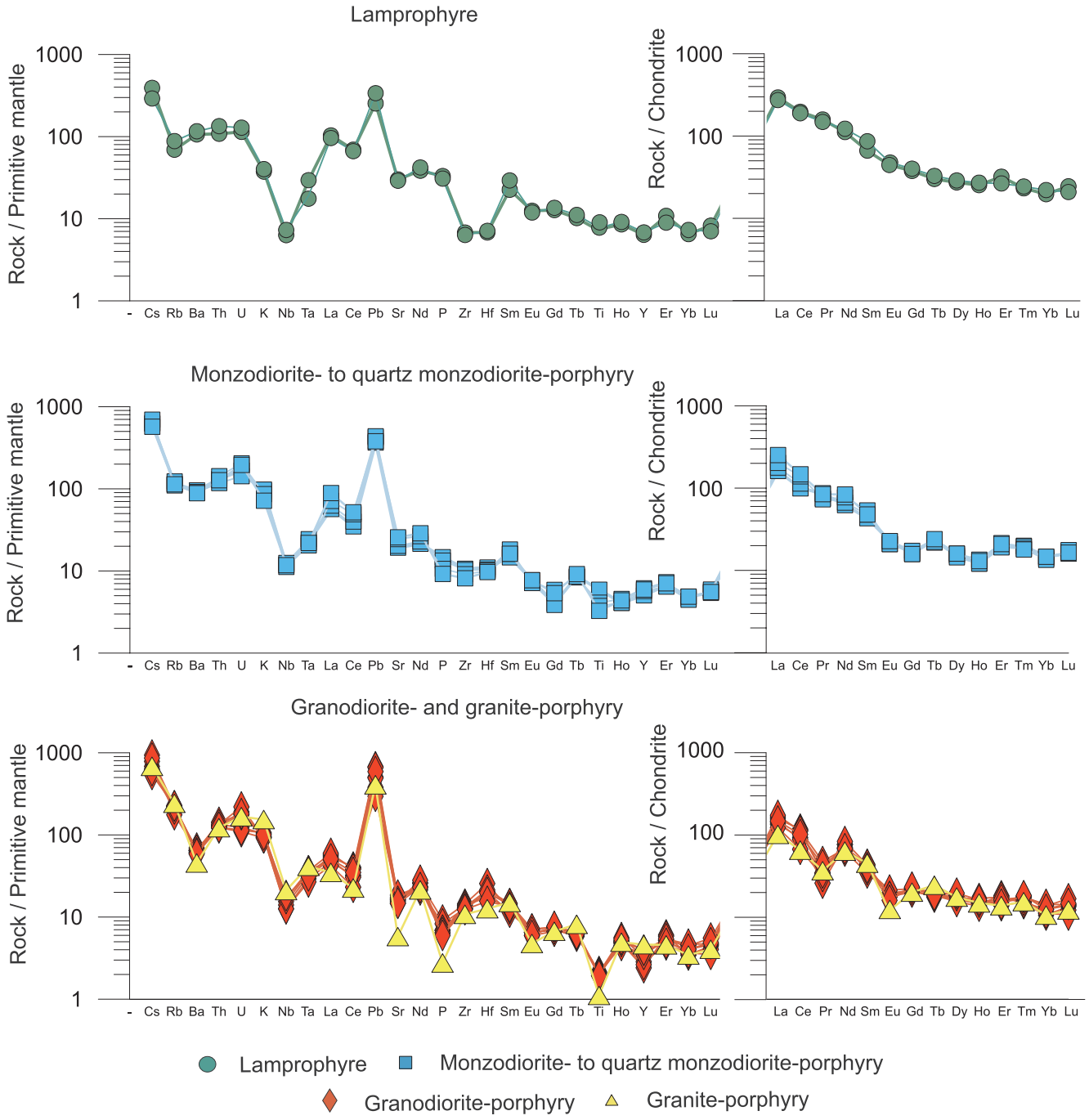

Fig. 13. Primitive mantle-normalized extended trace element spider diagrams (normalization with respect to Sun and McDonough, 1989) and rare earth element chondrite-normalized diagrams (normalization with respect to McDonough and Sun, 1995) for the igneous rock from the Agylki deposit. The individual rock compositions are from Table 2.

system. Overall, this is consistent with a common participation of mantle-derived, possibly potassic lamprophyric melts and crustal granitoid magmas in transitional weakly-reduced to weakly-oxidized, metaluminous to weakly peraluminous I- to hybrid I-S type igneous suites parental for reduced intrusion-related Au and W deposits (Hart et al., 2004a,b; Hart, 2007; Mair et al., 2006, 2011; Rasmussen et al., 2011). As emphasized by Rasmussen et al. (2011), Newberry and Swanson (1986) and Newberry (1998), "economic W deposits are not associated with magmas solely derived from partial melting of metasedimentary rocks, and true S-type magmas are not capable of producing economic W mineralization". Igneous association formed due to melting of different protoliths at different depths followed by nearly simultaneous intrusion of geochemically-contrasting magmas are common in collision-related orogenic systems; this process could correspond to a progressing ascent of hot asthenospheric material in a late- to post-collisional environment (e.g., Jahn et al., 2015). Larger granitoid intrusions (with more pronounced S-type signatures) found in the deposit area post-date reduced W skarn at Agylki and are accompanied by weak Sn-W mineralization. This corresponds to a generally later (than reduced W skarn deposits) development of Sn-W mineralization in collisional orogenic systems (Soloviev, 2008).

Various models of the magma mingling and mixing can be

suggested, particularly due to the presence of sharply zoned, locally resorbed, plagioclase phenocrysts and rounded (resorbed) quartz phenocrysts in granodiorite-porphyry (e.g., Hibbard, 1981). Thus, it can be speculated that the granodiorite magma itself may represent a product of mingling/mixing of more mafic and silicic magmas. This process could be affecting solubility of fluid species and metals in the magma, thus facilitating their transition to an exsolving hydrothermal fluid. This would particularly affect solubility of carbonic and other species (P, etc.) that are incompatible with granitoid compositions; this mechanism would be an efficient tool for liberating dissolved species specifically in view of insignificant degree of fractionation, the latter evidenced by relatively small Eu anomalies in the granodiorite-porphyry (Fig. 13; cf. Rasmussen et al., 2011). Nevertheless, progressing magmatic differentiation could be responsible for W accumulation in more fractionated rock varieties (Fig. 5F). Graphic and micropegmatitic quartz-feldspar intergrowths as well as microvugs filled with quartz, feldspars, and locally calcite observed in granodiorite-porphyry indicate that the magma has reached saturation in respect with water and possibly CO_2.

9.3. *Integrated vertical model of W skarn deposits: Structural and lithological aspects*

The structural setting of the Agylki deposit can be interpreted in the context of spatial evolution of various structural types of mineralized zones relative to a causative intrusion observed at W skarn deposits (Fig. 14). Specifically, it may correspond to an upper, most distal structural level occurring within 1–2 km above the main pluton contact, where igneous rocks form dike swarms and occasional small stocks, whereas larger intrusions are revealed by geophysical data at a depth. At this level, flat-lying ("stratified") lenticular and occasionally tabular skarn zones can be formed in flat-lying to shallow-dipping lithologies. Such flat-lying skarn zones are absent in steeper-dipping units, however, it appears that they may be associated with thrust-faults. Multiple "horizons" of lenticular mineralized skarn zones replacing favorable (Ca-rich) lithologies and alternating with barren layers can be formed. Notably the deposit remains underexplored due to insufficient depth of historical drill holes, which were terminated shortly after intersecting the mineralized skarn zone. Meantime, flat-lying mineralized skarn zones forming multi-level systems above an intrusion were demonstrated at the Skrytoe reduced W skarn deposit (e.g., Soloviev and Kryazhev, 2017). Distal shallow-dipping mineralized W skarn zones are also known at oxidized and redox-intermediate W skarn deposits such as Sangdong (South Korea; Kim et al., 1988).

Deeper, more proximal to a causative pluton, structural levels can comprise steep-dipping tabular skarn zones as well as various contact (frontal) lens-like and veined skarns evolving to, locally - branching and other complex-shaped skarn zones (Fig. 14). They are associated with steep pluton apophyses and stocks merging with the main pluton to a depth and/or by local fault zones, steep dike swarms and other features typically occurring above the main pluton. This complexity is further complicated at yet deeper levels by an increasingly complex shape of a

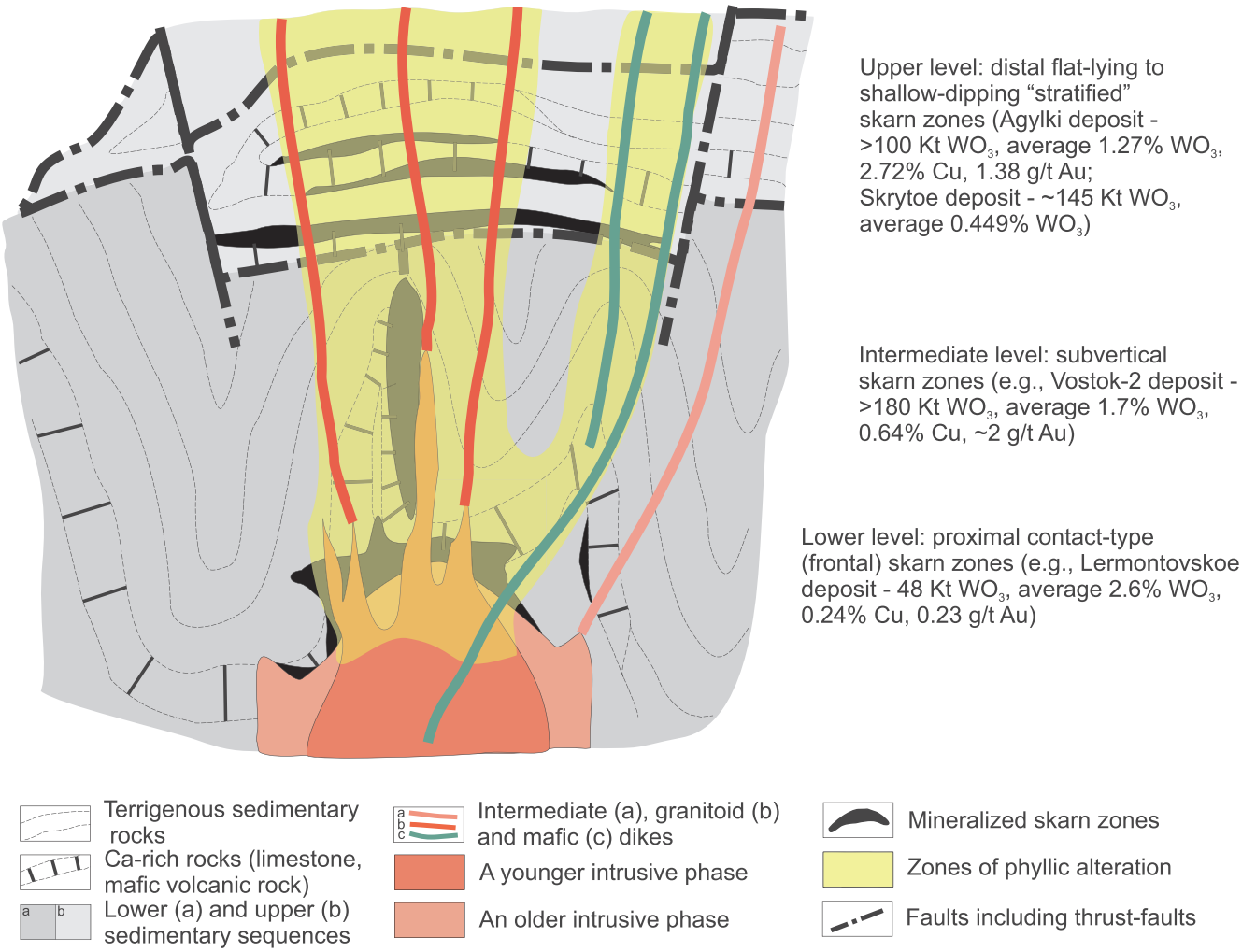

Fig. 14. Idealized model showing locations of various structural types of mineralized skarn zones relative to a causative intrusion (on the examples in the Eastern Russia).

multiphase pluton contact, with numerous roof pendants, crosscutting intrusive apophyses, dike swarms merging to and splitting of the main pluton, and other local features. Lens-shaped to tabular skarn zones can be formed in metasedimentary sequences comprising contrasting lithologies, particularly in steeply bedded units. Mineralized post-skarn hydrothermal alteration can be structurally focused within the same structures, thus further contributing to the overall metal grades. This is well presented at the Vostok-2 reduced W skarn deposit (Sikhote-Alin), where a subvertical skarn zone extends for over 1 km and is characterized by high W, Au, Cu and Bi grades (Soloviev and Krivoschekov, 2011; Soloviev et al., 2017a). The contact (frontal) skarn settings are also common at W skarn deposits including reduced W skarns such as Lermontovskoe (Sikhote-Alin, Russia; Soloviev et al., 2017b) and Ingichke (Uzbekistan; Soloviev and Kryazhev, 2018a), as well as at oxidized and redox-intermediate W skarn deposits such as Pine Creek (California; Newberry, 1982), Lyangar and Koitash (Uzbekistan; Soloviev and Kryazhev, 2018b, 2019) and others.

These structural settings appear to be principally aligned with the structural tension pattern occurring above a cooling intrusion (Soloviev, 2008) and correspond to an evolution from a conductive to convective intrusion-centered heat/fluid flow system (Johnson and Norton, 1985). However, at individual deposits, one or two settings (structural levels) typically occur, whereas all three settings are almost never present together. Further "reduction" of the vertical extent and limited variability of structural types of mineralized skarn zones occur in the host sequences with dominant either subhorizontal dip of sedimentary sequences (steep skarn zones are absent or negligible) or their steep dip (subhorizontal skarn zones are absent).

9.4. Magmatic-hydrothermal evolution

Crystallization magmatic differentiation was responsible for the progressive enrichment of the rocks in W (Fig. 5F) and increasing W accumulation in the residual magmatic melt (Newberry and Swanson, 1986; Newberry, 1998). In its evolution, the magmatic melt has reached saturation in water; this may have repeated at different intrusion phases thus causing cyclic/pulsed releases of magmatic-hydrothermal fluid, with correspondingly multiple development of hydrothermal alteration and related metal deposition (e.g., Li et al., 2017).

The fluid inclusions data (Table 4) indicate the involvement of low-carbonic aqueous, dominantly magnesian-sodic-chloride, moderately-saline (14.0–17.3 wt% NaCl-eq.), high-pressure (1.4 ± 0.2 kbars), moderately-hot (~400–500 °C) fluid (type 1 fluid inclusions) in the retrograde skarn formation at Agylki. This fluid could continue a trend from hotter, higher-pressure fluid originating directly from crystallizing magma at the prograde skarn stage (Fig. 15). No appreciable fluid enrichment in Ca is observed, unlike that reported at many other W skarn deposits (e.g., Kwak and Tan, 1981; Kwak, 1987); thus, fluid cooling could be the main factor causing scheelite precipitation in retrograde skarn at Agylki (Rafal'sky et al., 1984; Wood and Samson, 2000).

Similar low-carbonic, high-pressure (1.1–0.8 kbars), lower temperature (~300–400 °C) fluid conserved in type 2 fluid inclusions was responsible for the development of propylitic alteration assemblages. However, in contrast to the retrograde skarn fluid, the propylitic stage fluid was characterized by a strong enrichment in Ca. Propylitic alteration is a garnet/pyroxene-destructive process occurring after retrograde skarn alteration, principally in the form of an amphibole-chlorite-epidote-plagioclase-quartz ± sulfide assemblage (Zharikov, 1970; Einaudi et al., 1981; Newberry, 1982; Wilkinson et al., 2015). Intense replacement of skarn pyroxene by the amphibole-dominant propylitic assemblages could be the main mechanism of Ca sourcing into mineralizing fluid (e.g., Soloviev et al., 2017b). The elevated Ca content in type 2 inclusions indicates that, in addition to the fluid cooling, scheelite deposition could be affected by strong fluid enrichment in Ca, similarly to some other W skarn deposits (Kwak and Tan, 1981; Soloviev and Kryazhev, 2017b, Soloviev et al., 2017a,b). Sulfidation of pyroxene in reduced conditions results in the deposition of pyrrhotite (Burton et al., 1982; Gamble, 1982).

The early phyllic alteration assemblages at Agylki were formed from a boiling high-carbonic fluid, with subsequent fluid separation into yet a higher-carbonic gaseous phase (type 3A fluid inclusions) and a low-carbonic aqueous phase (type 3B fluid inclusions) (Table 4). An elevated carbonic and specifically methane content differs the fluids from those, which formed skarn and propylitic alteration assemblages, and indicates a new fluid influx from crystallizing magma (Fig. 15). A high carbonic content and the fluid enrichment in Au, As, Bi, Sb, Te, P suggest the fluid sourcing from a different, possibly mafic magma chamber, or the fluid release due to mingling/mixing of mafic and silicic magmas (cf. Rasmussen et al., 2011). There is a possibility of a long-lasting development of the mafic magma chamber(s) that remained active before, during and after the emplacement of granitic phases. This may have also caused the fluid enrichment in phosphorus, and phosphate complexes could have been played a strong role in W transport (Manning and Henderson, 1984), as evident by the association of scheelite with apatite. In contrast, W could be supplied from crystallizing silicic magma, as advanced magmatic differentiation promoted enrichment of residual melt in W (e.g., Newberry and Swanson, 1986; Newberry, 1998). A greater depth of fluid separation from

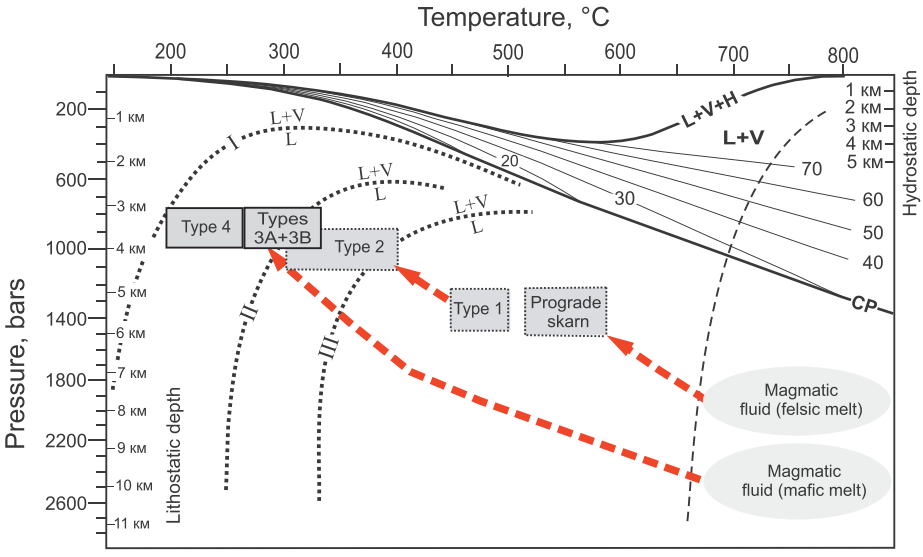

Fig. 15. Estimated pressure and temperature conditions and evolutional paths for different fluid inclusion types in hydrothermal assemblages at the Agylki deposit, with composition of different fluid inclusion types as a function of depth and temperature (the principal diagram after Bodnar et al., 1985; Fournier, 1999). Vapor-pressure curves for H_2O-NaCl solutions at 0–70 wt% NaCl-eq. and the three-phase (L + V + H) curve are shown after Atkinson (2002) and Becker et al. (2008). Dashed line represents line represents water-saturated granite solidus (Holtz et al., 2001). The two-phase (L/L + V) curves (dotted lines) for H_2O-NaCl-CO_2 fluid containing 6 wt% NaCl and 4.08 mol.% CO_2 (curve I), 10 mol.% CO_2 (curve II), and 21.33 mol.% CO_2 (curve III) (Schmidt and Bodnar, 2000) are presented. PT-fields for the major fluid inclusion types and possible evolutional paths for fluids (arrows) are shown. Due to lack of fluid inclusion data, the RT-field for the prograde skarn is shown conditionally.

magma (possibly corresponding to a deep-seated mafic magma chamber) is consistent with moderate to low (~320–280 °C) fluid temperatures at the level of mineralization, i.e., the fluids were cooled before reaching the mineral deposition level. Additional Ca sourcing could be also provided by replacement of Ca-plagioclase in igneous rocks by sericite (muscovite) and Na-plagioclase (albite). Fluid cooling and pH increase due to boiling (Drummond and Ohmoto, 1985) were affecting W solubility that, together with dissociation of Ca-bearing complexes liberating Ca, promoted scheelite deposition (Rafal'sky et al., 1984; Wood and Samson, 2000). High CO_2 and CH_4 are common in fluids at reduced intrusion-related Au deposits (e.g., McCoy et al., 1997; Lang and Baker, 2001; Baker, 2002) and in late fluids at reduced W skarn deposits (Fonteilles et al., 1989; Gerstner et al., 1989).

The late phyllic alteration assemblages comprising late sulfide and sulfosalt minerals were formed from a homogenous low-carbonic, moderately-saline (14.0–17.8 wt% NaCl-eq.) and low-temperature (~200–250 °C) fluid. This temperature range is consistent with the presence of native bismuth in this mineral assemblage ($T_{melting}$ = 271.4 °C). Au transport at low temperatures corresponding to phyllic alteration stage occurs mostly in the form of bisulfide rather than chloride complexes (e.g., Gammons and Williams-Jones, 1997). Consistently, following the native Bi/bismuthinite transition, transport by and precipitation of gold from bisulfide complexes was most intense due to reduced conditions and low salinity (low chloride content) of the fluids (e.g., Seward, 1991). Close association of Au and Bi minerals supports also possible scavenging of Au in Bi melt coexisting with the hydrothermal fluid (Tooth et al., 2008; Acosta-Gongora et al., 2015).

Overall, hydrothermal alteration and mineralization at Agylki occurred at lower temperatures, as compared to the other reduced W skarn deposits (e.g., Mathieson and Clark, 1984; Gerstner et al., 1989; Yuvan, 2006; Soloviev et al., 2017a,b, 2019; Soloviev and Kryazhev, 2017, 2018a). This is consistent with the lack of wollastonite in prograde calcic skarn, abundance of epidote and prehnite in propylitic alteration assemblages, and abundance of sphalerite and galena, together with Au, Te, Sb mineralization in phyllic alteration assemblages. This complements the respective structural setting of the Agylki deposit possibly corresponding to the most distal (from a causative pluton) level in the integrated model of skarn deposits. This would be also consistent with the dominant convective heat/fluid flow (Johnson and Norton, 1985) in the distal settings and may imply a greater involvement of meteoric water during the deposit formation.

9.5. Tungsten-gold association: regional context

The location of the Agylki W skarn deposit in an Au-dominant metallogenic province and presence of Au mineralization at the deposit suggest some regional- to local-scale genetic links of W and Au mineralization. This is supported by compositional similarity and coeval age of the granitoid dikes at Agylki and the main Au deposits in the region. Many Au-dominant deposits contain minor scheelite mineralization.

In particular, in the South Verkhoyansk metallogenic zone that possibly extends over the Tompon metallogenic zone further to the southeast, minor scheelite is present at the large (> 500 t Au, average 5.1 g/t Au) Nezhdaninskoe Au deposit (Fig. 2). The deposit is represented by mineralized veins and linear stockwork zones that follow tectonized zones and/or are coincident with altered dikes intruding Permian and Lower Triassic terrigenous rocks. Two dike suites are distinguished at the deposit, namely, (1) a Late Jurassic-Early Cretaceous suite of gabbro-diorite and diorite-porphyry (154–140 Ma), and (2) an Early-early Late Cretaceous shoshonitic lamprophyre suite (131–94 Ma after Bortnikov et al., 1998; 121 ± 1 Ma by U-Pb method on zircons, after Chernyshev et al., 2012). Correspondingly, two main mineralizing events are distinguished including (1) the early weakly auriferous pyrite-arsenopyrite event, locally with scheelite, occurring after the gabbro-diorite and diorite-porphyry dikes, and (2) the late, most productive, Au-sulfide-sulfosalt event (with Bi, Ag, Sb minerals) occurring after the shoshonitic lamprophyre dikes (Indolev, 1979) at 124–105 Ma (Bortnikov et al., 1998).

Significant scheelite mineralization is also present at some Au deposits in the Yana-Kolyma metallogenic belt, where a distinct group of Au deposits is distinguished as the intrusion-related Au-Bi deposits or "Au-rare metal deposits" (Gamyanin et al., 2000; Volkov et al., 2007; Goryachev and Gamyanin, 2006; Voroshin et al., 2014; Vikent'eva et al., 2018). These Au deposits are related to the Late Jurassic-Early Cretaceous I-type, ilmenite-series granitoid suites (typically dikes and small stocks) (Goryachev, 1998, 1999; Goryachev and Pirajno, 2014; Vikent'eva et al., 2018). In particular, scheelite mineralization was reported at the large (~100 t Au, average 7.7 g/t Au) Chepak Au deposit considered within this group (Fig. 1). This deposit is represented by numerous auriferous quartz-sericite veins and related zones of phyllic alteration that are associated with granodiorite and granite-porphyry dikes assigned to the Nera-Bokhapchin and/or Basugunyin dike suites. Muscovite/sericite from the mineralized veins yielded the Ar-Ar radiologic age of 146.5 Ma (Goryachev, 1998). Arsenopyrite and loellingite are the dominant sulfide/arsenide minerals and typically form over 50 vol%, locally up to 80–90 vol% of the mineralized veins. Scheelite is ubiquitous in the veins (0.5–1 vol%), and the deposit contains about 6 Kt WO_3 (average 0.06% WO_3). Other typical minerals include native Bi, bismuthinite, tetradymite, and tellurobismuthite. Both sulfide-related (fine-dispersed) and native gold (fineness 850-970‰) are present (Volkov et al., 2007).

Overall, these signatures support possible genetic links of reduced W skarn and vein/stockwork Au(± W) deposits within a broader regional-scale magmatic-hydrothermal system, where reduced W skarn deposits are formed in favorable (Ca-rich) lithologies and contain minor Au mineralization, whereas intrusion-related Au(± W) deposits locally contain minor W mineralization. Notably scheelite occurs at Au deposits containing abundant As and Bi minerals. It further appears that, whereas minor Au mineralization can occur in paragenesis with scheelite at W skarn deposits, most significant Au mineralization postdates scheelite-bearing mineralizing stages at the Au-dominant deposits. On the other hand, there could be some differences in coeval but compositionally distinct fertile igneous suites, as it is suggested for the Tungsten, Mayo, and Tombstone plutonic suites in similar tectonic and metallogenic settings of Yukon-Alaska, with respectively different (W-dominant vs. Au-dominant) reduced intrusion-related mineralization styles (e.g., Hart et al., 2004a,b).

10. Conclusions

The Agylki deposit is a large (and possibly underexplored) and high-grade reduced W (W-Cu-Au-Bi) skarn deposit that may represent part of an unrecognized W-Au metallogenic belt. The latter extends along the Verkhoyansk fold-and-thrust belt, which occurs in the outer part of the Verkhoyansk-Kolyma orogenic system and was formed after a passive continental margin adjoining the Siberian craton. The belt roughly parallels the main metallogenic belts of the region comprising numerous gold (Au, Au-Bi, Au-Sb, etc.) and W-Sn deposits. The deposit is related to a swarm of Late Jurassic-Early Cretaceous monzodiorite-porphyry to granitoid (granodiorite- to granite-porphyry) dikes that intrude a Triassic terrigenous sequence.

The dikes comprise weakly reduced-weakly oxidized (ilmenite-titanite-bearing), high- to medium-K calc-alkaline, metaluminous to weakly peraluminous, I-type rocks. The presence of igneous rocks with contrasting composition may indicate different magma sources, with further mingling/mixing of different magmas. This process could be affecting solubility of fluid species and metals in the magma, thus facilitating their transition to an exsolving hydrothermal fluid. This would particularly affect solubility of carbonic and other species (P, etc.) that are incompatible with granitoid compositions; this mechanism would be an efficient tool for liberating dissolved species specifically in view of a weak fractionation, the latter evidenced by

relatively small Eu anomalies in the granodiorite-porphyry. However, progressing magmatic differentiation could be responsible for W accumulation in more fractionated rock varieties.

The deposit is represented by a single lenticular flat-lying to shallow-dipping mineralized zone that was formed by the replacement of a limestone horizon found in the Triassic terrigenous sequence. This may correspond to a distal level in an integrated structural model of W skarn deposits that occurs well above causative pluton. The deposit bears signatures of reduced W skarn deposits, with dominant pyroxene (hedenbergite-enriched) skarn containing pyrrhotite and scheelite. Propylitic alteration assemblages (amphibole-chlorite-epidote-calcite-quartz with abundant pyrrhotite, scheelite and minor chalcopyrite) overprint skarn and are in turn overprinted by zones of phyllic alteration (quartz-sericite-Fe-carbonate) comprising abundant apatite and arsenopyrite followed by scheelite, chalcopyrite and other sulfides as well as Bi, Te and Au minerals.

Fluid inclusions data indicate formation of retrograde (mainly pyroxene-quartz-amphibole) skarn from aqueous, dominantly magnesian-sodic-chloride, moderate-salinity (14.0–17.3 wt% NaCl-eq.), high pressure (1.4 ± 0.2 kbars), moderately-hot (~400–500 °C) fluid. Propylitic alteration assemblages were formed from homogenous, low-carbonic, lower salinity (8.8–13.7 wt% NaCl-eq.), lower pressure (1.1–0.8 kbars) and lower temperature (~300–400 °C) Ca-enriched fluid. Early phyllic alteration assemblages were formed from a boiling fluid, with separation of carbonic-rich (particularly methane-enriched) gaseous fluid and coexisting low-carbonic aqueous fluid at ~320–280 °C and ~0.9 ± 0.1 kbar. Late phyllic alteration assemblages were formed from homogenous, low-carbonic, moderate-salinity (14.0–17.8 wt% NaCl-eq.) low-temperature (250–200 °C) fluid. Fluid cooling and pH increase due to boiling were affecting W solubility that, together with dissociation of Ca-bearing complexes liberating Ca, promoted scheelite deposition.

The deposit could be part of a broader regional-scale magmatic-hydrothermal system comprising almost coeval intrusion-related reduced W skarn deposits and vein/stockwork Au(± W) deposits. However, there could be some differences in coeval but compositionally distinct igneous suites, with respectively different (W-dominant vs. Au-dominant) reduced intrusion-related mineralization styles.

Acknowledgments

This paper represents part of the authors' work on research and assessment of W, Au, Cu and other deposits. The work was completed under financial support from the Scientific Program of the IGEM RAS. Editorial reviews by Huayong Chen, Reimar Seltmann, Dmitry Konopelko and an anonymous reviewer significantly improved the paper.

Appendix A. Supplementary data

Supplementary data to this article can be found online at https://doi.org/10.1016/j.oregeorev.2020.103452.

References

Acosta-Gongora, P., Gleeson, S.A., Samson, I.M., Ootes, L., Corriveau, L., 2015. Gold refining by bismuth melts in the iron oxide-dominated NICO Au-Co-Bi (± Cu ± W) deposit, NWT, Canada. Econ. Geol. 110, 291–314.

Akinin, V.V., Prokopiev, A.V., Toro, J., Miller, E.L., Wooden, J., Goryachev, N.A., Alshevsky, A.V., Bakharev, A.G., Trunilina, V.A., 2009. U-Pb SHRIMP age of granitoids from the Main Batholith Belt (North East Asia). Dokl. Earth Sci. 426, 605–610.

Amuzinsky V.A., 1974. Gold and antimony mineralization in the western part of the Tompon ore zone. In: Ore Mineralization of Yakutia. Yakutian Branch of the Science Academy of the USSR, Yakutsk, pp. 35–46 (in Russian).

Atkinson, A.B., 2002. A Model for the PTX Properties of H_2O-NaCl. M.Sc. Thesis. Virginia Tech. Institute and State University, pp. 126.

Baker, T., 2002. Emplacement depth and carbon dioxide-rich fluid inclusions in intrusion-related gold deposits. Econ. Geol. 97, 1111–1117.

Baker, T., Pollard, P.J., Mustard, R., Mark, G., Graham, J.L., 2005. A comparison of granite-related tin, tungsten, and gold-bismuth deposits: implications for exploration. SEG Newslett. 61, 5–17.

Bakker, R.J., 2003. Package FLUIDS 1. Computer programs for analysis of fluid inclusions data and for modeling bulk fluid properties. Chem. Geol. 194, 3–23.

Becker, S.P., Fall, A., Bodnar, R.J., 2008. Synthetic fluid inclusions. XVII. PVTX properties of high-salinity H_2O-NaCl solutions (> 30 wt.% NaCl): applications to fluid inclusions that homogenize by halite disappearance from porphyry copper and other hydrothermal ore deposits. Econ. Geol. 103, 539–544.

Bilinkis G.M., 1961. Report on the exploration for tungsten and copper at the Agylki deposit in 1966-1970. Unpubl. Prof. Report. Soviet Ministry of Geology, Yakutsk-Moscow. (in Russian).

Bodnar RJ., Vityk M.O., 1994. Interpretation of microthermometric data for H2O-NaCl fluid inclusions. In: De Vivo B., Frezzotti M.L. (Eds.) Fluid Inclusions in Minerals, Methods and Applications. Blacksburg, Virginia Tech, pp. 117–130.

Bodnar, R.J., Burnham, C.W., Sterner, S.M., 1985. Synthetic fluid inclusions in natural quartz. III. Determination of phase equilibrium properties in the system H_2O-NaCl to 1000°C and 1500 bars. Geochim. Cosmochim. Acta 49, 1861–1873.

Bortnikov, N.S., Gamyanin, G.N., Alpatov, V.A., Naumov, V.B., Nosik, L.P., Mironova, O.F., 1998. Mineralogy, geochemistry and origin of the Nezhdaninsk gold deposit (Sakha-Yakutia, Russia). Geol. Ore Deposits 40 (2), 121–138.

Bortnikov, N.S., Gamynin, G.N., Vikenteva, O.V., Prokofev, V.Y., Prokopev, A.V., 2010. The Sarylakh and Sentachan gold–antimony deposits, Sakha-Yakutia: A case of combined mesothermal gold–quartz and epithermal stibnite ore. Geol. Ore Deposits 52 (5), 339–372.

Bowman, J.R., Covert, J.J., Clark, A.H., Mathieson, G.A., 1985. The CanTung E-Zone scheelite skarn orebody, Tungsten, Northwestern Territories: oxygen, hydrogen and carbon isotope studies. Econ. Geol. 80, 1872–1895.

Burruss R.C., 1981. Analysis of phase equilibria in C-O-H-S fluid inclusions: in Hollister L. S., Crawford M.L., eds., Fluid inclusions: Application to Petrology. Min Assoc Canada Short Course Handbook, Calgary 6, pp. 39–74.

Burt, D.M., 1977. Mineralogy and petrology of skarn deposits. Soc. Italiana Mineralogia Petrologia Rend. 33, 859–873.

Burton, J.C., Taylor, L.A., Chou, I.-M., 1982. The f_{O2}-T and f_{S2}-T stability relations of hedenbergite and of hedenbergite-johannsenite solid solutions. Econ. Geol. 77, 764–783.

Chappell, B.W., Bryant, C.J., Wyborn, D., 2012. Peraluminous I-type granites. Lithos 153, 142–153.

Chappell B.W., White A.J.R., 1992. I- and S-type granites in the Lachlan Fold Belt. Trans. Royal Soc. Edinburgh, Earth Sciences 83, pp. 1–26.

Chernyshev, I.V., Bakharev, A.G., Bortnikov, N.S., Goltsman, Y.V., Kotov, A.B., Gamyanin, G.N., Chugaev, A.V., Salnikova, E.B., Bairova, E.D., 2012. Geochronology of igneous rocks at and near to the Nezhdaninka gold deposit, Yakutia, Russia: U-Pb, Rb–Sr, and Sm–Nd isotopic data. Geol. Ore Deposits 54 (6), 411–433.

Crawford M.L., 1981. Phase equilibria in aqueous fluid inclusions. In: Hollister L.S., Crawford M.L. (Eds) Fluid inclusions: Application to Petrology. Min. Assoc. Canada Short Course Handbook, Calgary 6, pp.75–100.

Dick, L.A., Hodgson, C.J., 1982. The MacTung W-Cu(Zn) contact metasomatic and related deposits of the North-eastern Canadian Cordillera. Econ. Geol. 77, 845–867.

Dorofeev D.A., 1961. One of types of tungsten deposits in Eastern Yakutia. In: Materials on Geology and Mineral Deposits of Yakutian SSR. V. 5. Gosgeoltechizdat Publishing, Moscow, pp.12-31 (in Russian).

Drummond, E., Ohmoto, H., 1985. Chemical evolution and mineral deposition in boiling hydrothermal systems. Econ. Geol. 80, 126–147.

Einaudi, M.T., Meinert, L.D., Newberry, R.J., 1981. Skarn deposits. Econ. Geol. 75, 317–391.

Flerov, B.L., Bichyus, B.Y., Korostelev, V.I., 1974. The skarn tungsten-copper deposit. In: Flerov, B.L. (Ed.), Mineralogy of Endogenous Deposits in Yakutia. Nauka Publishing, Novosibirsk, pp. 41–64 (in Russian).

Fonteilles, M., Soler, P., Demange, M., Derre, C., Krier-Schellen, A.D., Verkaeren, J., Guy, B., Zahm, A., 1989. The scheelite skarn deposit of Salau (Ariege, French Pyrenees). Econ. Geol. 84, 1172–1209.

Fournier, R.O., 1999. Hydrothermal process related to movement of fluid from plastic into brittle rock in the magmatic-epithermal environment. Econ. Geol. 94, 1193–1212.

Fridovsky V.Y., 2002. Structures of gold fields and deposits in the Yana-Kolyma ore belt. In: Metallogeny of Collisional Geodynamic Environments. Vol. 1. 410 p. (in Russian).

Fridovsky, V.Y., 2018. Structural control of orogenic gold deposits of the Verkhoyansk-Kolyma folded region, northeast Russia. Ore Geol. Rev. 103, 38–55.

Frost, B.R., Barnes, C.G., Collins, W.J., Arculus, R.J., Ellis, D.J., Frost, C.D., 2001. A geochemical classification for granitic rocks. J. Petrology 42, 1771–1802.

Gamble, R.P., 1982. An experimental study of sulfidation reaction involving andradite and hedenbergite. Econ. Geol. 77, 784–797.

Gammons, C.H., Williams-Jones, A.E., 1997. Chemical mobility of gold in the porphyry-epithermal environment. Econ. Geol. 92, 45–59.

Gamyanin, G.N., Goncharov, V.I., Goryachev, N.A., 2000. Gold-rare metal deposits of Northeast Russia. Russian J. Pacific Geol. 15, 619–636 (in Russian).

Gerstner, M.R., Bowman, J.R., Pasteris, J.D., 1989. Skarn formation at the McMillan Pass tungsten deposit (MacTung), Yukon and Northwest territories. 1. P-T-X-V characterization of the methane-bearing, skarn-forming fluids. Can. Miner. 27, 545–563.

Goldfarb, R., Taylor, R.D., Collins, G.S., Goryachev, N.A., Orlandini, O.F., 2014. Phanerozoic continental growth and gold metallogeny of Asia. Gondwana Res. 25, 48–102.

Goryachev, N.A., 1998. Geology of Mesozoic Gold-Quartz Vein Belts of Northeast Asia. NEISRI FEB RAS, Magadan (in Russian).

Goryachev, N.A., 1999. Geology and genesis of the Mesozoic gold-quartz veined belts in the Asian Northeast. D.Sc. Dissertation, Magadan. 444 p. (in Russian).

Goryachev, N.A., Gamyanin, G.N., 2006. Gold–bismuth (gold-rare metal) deposits of North East Russia: Types, and exploration perspectives. In: Gold Ore Deposits of East Russia. NESC FEB RAS, Magadan, pp. 50–62 (in Russian).
Goryachev, N.A., Pirajno, F., 2014. Gold deposits and gold metallogeny of Far East Russia. Ore Geol. Rev. 59, 123–151.
Goryachev, N.A., Shpikerman, V.I., Church, S.E., Gvozdev, V.I., 2018. Calcic skarn ore deposits of the North-East Russia. Ore Geol. Rev. 103, 3–20.
Gustafson, W.I., 1974. The stability of andradite, hedenbergite, and related minerals in the system Ca-Fe-Si-O-H. J. Petrol. 15, 455–496.
Guy, B., Faure, N., Le Loch, G., Varenne, J.-L., 1988. Etude microtermometrique des inclusions fluids des skarns a tungstene de Costabonne (Pyrenees, France): quelques resultants. C.R. Acad. Sci. Ser. II 307, 33–38.
Gvozdev, V.I., 2002. The Lead-Antimony–Bismuth Mineralization in Ores of the Agylki Skarn–Scheelite–Sulfide Deposit (Yakutiya, Russia). Geol. Ore Deposits 44 (4), 300–311.
Gvozdev, V.I., 2010. Ore-magmatic Systems of Skarn Scheelite-sulfide Deposits of the Russian Far East. Dalnauka Publishing, Vladivostok (in Russian).
Hart C.J.R., 2007. Reduced intrusion-related gold systems. In Goodfellow W.D. (ed.) Mineral deposits of Canada: A synthesis of major deposit types, district metallogeny, the evolution of geological provinces, and exploration methods. Geol. Assoc. Canada, Mineral Deposits Division, Spec. Publ. 5, pp. 95–112.
Hart, C.J.R., Goldfarb, R.J., Lewis, L.L., Mair, J.L., 2004a. The northern cordilleran mid-Cretaceous plutonic province: ilmenite/magnetite-series granitoids and intrusion-related mineralization. Resour. Geol. 54, 253–280.
Hart, C.J.R., Mair, J.L., Goldfarb, R.J., Groves, D.I., 2004b. Source and redox controls on metallogenic variations in intrusion-related ore systems, Tombstone Tungsten Belt, Yukon Territory, Canada. Trans Roy. Soc. Edinburgh, Earth Sci. 95, 339–356.
Hibbard, M.J., 1981. The magma mixing origin of mantled feldspars. Contrib. Miner. Petrol. 76, 158–170.
Holtz, F., Becker, A., Freise, M., Johannes, W., 2001. The water-undersaturated and dry Qz-Ab-Or system revisited. Experimental results at very low water activities and geological implications. Contrib. Miner. Petrol. 141, 347–357.
Indolev, L.N., 1979. Dikes in Ore Districts of Eastern Yakutia. Nauka Publishing, Moscow, pp. 196.
Ishihara, S., 1981. The granitoid series and mineralization. Econ. Geol. 75, 458–484.
Ishihara, S., 2004. The redox state of granitoids relative to tectonic setting and earth history: the magnetite-ilmenite series 30 years after. GSA Spec. Paper 389, 23–33.
Jahn, B., Valui, G., Kruk, N., Gonevchuk, V., Usuki, M., Wu, J.T.J., 2015. Emplacement ages, geochemical and Sr–Nd–Hf isotopic characterization of Mesozoic to early Cenozoic granitoids of the Sikhote-Alin orogenic belt, Russian Far East: crustal growth and regional tectonic evolution. J. Asian Earth Sci. 111, 872–918.
Johnson, J.W., Norton, D., 1985. Theoretical prediction of hydrothermal conditions and chemical equilibria during skarn formation in porphyry copper systems. Econ. Geol. 80, 1797–1823.
Jowett E.C., 1991. Fitting iron and magnesium into the hydrothermal chlorite geothermometer. GAC/MAC/SEG Joint Annual Meeting (Toronto). Program with Abstracts 16, p. 62.
Khanchuk, A.I., Kemkin, I.V., Kruk, N.N., 2016. The Sikhote-Alin orogenic belt, Russian South East: terranes and the formation of continental lithosphere based on geological and isotopic data. J. Asian Earth Sci. 120, 117–138.
Khudoley A.K., 2003. Tectonics of passive margins of ancient continents: Examples of the eastern margin of the Siberian craton and western margin of the North American craton. D.Sc. Thesis, St-Petersburg State Univ./VSEGEI. p. 36. (in Russian).
Kim, K.H., Kim, J.J., Nakai, N., Lee, H.J., 1988. Stable isotope studies of the Sangdong tungsten ore deposit, South Korea. Mining Geol. 38 (6), 473–487.
Kwak, T.A.P., 1987. W-Sn Skarn Deposits and Related Metamorphic Skarns and Granitoids. Elsevier, Amsterdam, Oxford and New York, pp. 451.
Kwak, T.A.P., Tan, T.H., 1981. The importance of $CaCl_2$ in fluid composition trends – evidence from the King Island (Dolphin) skarn deposit. Econ. Geol. 76, 955–960.
Kwak, T.A.P., White, A.J.R., 1982. Contrasting W-Cu-Mo and W-Sn-F skarn types and related granitoids. Mining Geol. 32, 339–351.
Lang, J.R., Baker, T., 2001. Intrusion-related gold systems: the present level of understanding. Miner. Deposita 36, 477–489.
Layer, P.W., Newberry, R., Fujita, K., Parfenov, L.M., Trunilina, V.A., Bakharev, A.G., 2001. Tectonic setting of the plutonic belts of Yakutia, northeast Russia, based on $^{40}Ar/^{39}Ar$ geochronology and trace element geochemistry. Geology 29 (2), 167–170.
Le Maitre, R.W., Bateman, P., Dudek, A., Keller, J., Lameyre, J., Le Bas, M.J., Sabine, P.A., Schmid, R., Sorensen, H., Streckeisen, A., Wooley, A.R., Zanettin, B., 1989. A Classification of Igneous Rocks and Glossary of Terms. Blackwell, Oxford, pp. 193.
Li, Y., Selby, D., Condon, D., Tapster, S., 2017. Cyclic magmatic-hydrothermal evolution in porphyry systems: high-precision U-Pb and Re-Os geochronology constraints from the Tibetan Qulong porphyry Cu-Mo deposit. Econ. Geol. 112, 1419–1440.
Liou, J.G., 1993. Stability of natural epidotes. In: Hock, V., and Koller, F. (Eds.), 125 years Knappenwand. Proc. Symp., Salzburg/Austria, September 1990. Band 49, pp. 7–16.
Mair, J.L., Goldfarb, R.J., Johnson, C.A., Hart, C.J.R., Marsh, E.E., 2006. Geochemical constraints on the genesis of the Scheelite Dome intrusion-related gold deposit, Tombstone gold belt, Yukon, Canada. Econ. Geol. 101, 523–553.
Mair, J.L., Farmer, G.L., Groves, D.I., Hart, C.J.R., Goldfarb, R.J., 2011. Petrogenesis of mid-Cretaceous post-collisional magmatism at Scheelite Dome, Yukon, Canada: evidence for a lithospheric mantle source for intrusion-related gold systems. Econ. Geol. 106, 451–480.
Manning, D.A.C., Henderson, P., 1984. The behavior of tungsten in granitic melt-vapor systems. Contrib. Miner. Petrol. 86, 286–293.
Maniar, P.D., Piccoli, P.M., 1989. Tectonic discrimination of granitoids. Geol. Soc. Amer. Bull. 101, 635–643.
Mathieson, G.A., Clark, A.H., 1984. The CanTung E-Zone scheelite skarn orebody, Tungsten, Northwest Territories: a revised genetic model. Econ. Geol. 79, 883–901.
McCoy, D., Newberry, R.J., Layer, P., DiMarchi, J.J., Bakke, A., Masterman, J.S., Minehane, D.L., 1997. Plutonic-related gold deposits of Interior Alaska. Econ. Geol. Monogr. 9, 191–241.
McDonough, W.F., Sun, S.-S., 1995. The composition of the Earth. Chem. Geol. 120, 223–253.
Meinert, L.D., 1992. Skarns and skarn deposits. Geosci. Can. 19, 145–162.
Meinert, L.D., 1995. Compositional variations of igneous rocks associated with skarn deposits – chemical evidence for a genetic connection between petrogenesis and mineralization. In: Thompson, J.F.H. (Ed) Magmas, Fluids, and Ore Deposits. Min. Assoc. Canada Short Course Series 23, pp.401–418.
Meinert L.D., Dipple G.M., Nicolesku S., 2005. World skarn deposits. Econ. Geology 100th Anniv. Vol., 299–336.
Middlemost E.A.K., 1997. Magmas, Rocks and Planetary Development. Longman, Harlow. p. 299.
Naiborodin, V.I., 1959. Mineralogy and ore genesis of the Agylkinskoye deposit. Proc.VNI I-1, Vol. XIV, Issue 50. Magadan, p. 289–311 (in Russian).
Nelson, J., Colpron, M., 2007. Tectonics and metallogeny of the British Columbia, Yukon and Alaska Cordillera, 1.8 Ga to present. In: Goodfellow, W.D. (Ed.), Mineral Resources of Canada: A Synthesis of Major Deposit-types, District Metallogeny, the Evolution of Geological Provinces, and Exploration Methods: Geological Association of Canada Special Publication, 5, pp. 755–792.
Newberry, R.J., 1982. Tungsten-bearings skarns of the Sierra Nevada: 1. The Pine Creek mine, California. Econ. Geol. 77, 823–844.
Newberry, R.J., 1983. The formation of subcalcic garnet in scheelite-bearing skarns. Can. Miner. 21, 529–544.
Newberry R.J., 1998. W- and Sn-skarn deposits: a 1998 status report. In Lentz D.R. (Ed.) Mineralized intrusion-related skarn systems. Mineral. Assoc. Canada Short Course 26, pp. 289–335.
Newberry, R.J., Swanson, S.E., 1986. Scheelite skarn granitoids: an evaluation of the roles of magmatic source and process. Ore Geol. Rev. 1, 57–81.
Nikonov V.N., 2004. Geological setting, metallogeny and criteria for complex ore evaluation in the northern part of the Upper-Indigirka district. Ph.D. Thesis, MGPU. 36 p. (in Russian).
Nokleberg, W.J., Parfenov, L.M., Monger, J.W.H., Norton, I.O., Khanchuk, A.I., Stone, D.B., Scholl, D.W., Fujita, K., 1998. Phanerozoic tectonic evolution of the Circum-North Pacific. US Department of the Interior. Open-File Report 98–574. U.S. Geological Survey 125, p.
Parfenov, L.M., 1995. Terranes and the history of the Mesozoic orogenic belt formation in East Yakutia. Russian J. Pacific Geol. 14 (6), 32–43 (in Russian).
Parfenov, L.M., Kuzmin, M.I. (Eds.), 2001. Tectonics, Geodynamics and Metallogeny of the Sakha Republic (Yakutia). MAIK Nauka/Interperiodika, Moscow. 571 p. (in Russian).
Pearce, J., 1996. Sources and settings of granitic rocks. Episodes 19, 120–125.
Peccerillo, A., Taylor, S.R., 1976. Geochemistry of Eocene calc-alkaline volcanic rocks from the Kastamonu area, Northern Turkey. Contrib. Miner. Petrol. 58, 63–81.
Prokopiev, A.V., Pavlova, G.G., Borisenko, A.S., Travin, A.V., Toro, H., Tretyakov, F.F., Zaitsev, A.I., Bakharev, A.G., Trunilina, V.A., Vasiliev,D.A., Roev, S.P., 2010. Dikes and plutons of transverse magmatic belts in the Verkhoyansk fold-and-thrust belt: new geochronological data and their geodynamic implications. In: Tectonics and Geodynamics of Phanerozoic Orogens. GEOS, Moscow, Book II, pp. 174–177 (in Russian).
Protopopov R.I., Truschelev A.M., Protopopov G.H., Fedorova S.S., Scherbakov O.I., Kutygin R.B., Zharikova L.P., Budnikov I.V., Smetannikova L.I., Yuganova L.A., Fedorova S.Y., Schepelev N.G., 2016. The State Geological Map of the Russian Federation, 1:1000000 scale, Verkhiyansk-Kolyma series. Map sheet Q-53 – Verkhoyansk. Explanatory Notes. VSEGEI, St-Petersburg. P. 415. (in Russian).
Rafal'sky, R.P., Bryzgalin, O.V., Fedorov, P.L., 1984. Tungsten migration and scheelite deposition under hydrothermal conditions. Geochem. Internat. 21, 1–13.
Rasmussen K.L., 2013. The timing, composition, and petrogenesis of syn- to postaccretionary magmatism in the Northern Cordilleran miogeosyncline, Eastern Yukon and Southwestern Northwest Territories. Ph.D. Dissertation, The University of British Columbia, Vancouver. p. 810.
Rasmussen, K.L., Lentz, D.R., Falck, H., Pattison, D.R.M., 2011. Felsic magmatic phases and the role of late-stage aplitic dikes in the formation of the world-class CanTung tungsten skarn deposit, Northwest Territories, Canada. Ore Geol. Rev. 41, 75–111.
Roedder, E., 1984. Fluid inclusions in minerals. Rev. Mineral. 12, 644 p.
Sato, K., 1980. Tungsten skarn deposit of the Fujigatani mine, Southwest Japan. Econ. Geol. 75, 1066–1082.
Schmidt, C., Bodnar, R.J., 2000. Synthetic fluid inclusions: XVI. PVTX properties in the system H_2O-NaCl-CO_2 at elevated temperatures, pressures, and salinities. Geochim. Cosmochim. Acta 64, 3853–3869.
Seltmann, R., Soloviev, S., Shatov, V., Pirajno, F., Cherkasov, S., Naumov, E., 2010. Metallogeny of Siberia: Tectonic, geologic and metallogenic setting and significant deposits. Aust. J. Earth Sci. 57 (6), 655–706.
Seward, T.M., 1991. The hydrothermal geochemistry of gold: In: Foster, R.P. (Ed.) Gold Metallogeny and Exploration: Glasgow, Blackies, pp. 165–209.
Soloviev, S.G., 2008. Metallogeny of Phanerozoic Tungsten Skarn Deposits. Scientific World Publishing, Moscow, pp. 368 (in Russian).
Soloviev, S.G., Krivoschekov, N.N., 2011. The Vostok-2 gold-base metal-tungsten skarn deposit, Central Sikhote-Alin, Russia. Geol. Ore Deposits 6, 543–568.
Soloviev, S.G., Kryazhev, S.G., 2017. Geology, mineralization, and fluid inclusion characteristics of the Skrytoe reduced-type W skarn and stockwork deposit, Sikhote-Alin, Russia. Miner. Deposita 52 (6), 903–928.
Soloviev, S.G., Kryazhev, S.G., 2018a. Tungsten mineralization in the Tien Shan Gold Belt: geology, petrology, fluid inclusion, and stable isotope study of the Ingichke

reduced tungsten skarn deposit, western Uzbekistan. Ore Geol. Rev. 101, 700–724.
Soloviev, S.G., Kryazhev, S.G., 2018b. Magmatic-hydrothermal evolution at the Lyangar redox-intermediate tungsten-molybdenum skarn deposit, western Uzbekistan, Tien Shan: Insights from igneous petrology, hydrothermal alteration, and fluid inclusion study. Lithos 316–317, 154–177.
Soloviev, S.G., Kryazhev, S.G., 2019. Geology, mineralization, and fluid inclusion characteristics of the Koitash W-Mo skarn and W-Au stockwork deposit, Western Uzbekistan, Tien Shan. Miner. Deposita 54 (8), 1179–1206.
Soloviev, S.G., Kryazhev, S.G., Dvurechenskaya, S.S., 2017a. Geology, mineralization, stable isotope, and fluid inclusion characteristics of the Vostok-2 reduced W-Cu skarn and Au-W-Bi-As stockwork deposit, Sikhote-Alin, Russia. Ore Geol. Rev. 86, 338–365.
Soloviev, S.G., Kryazhev, S.G., Dvurechenskaya, S.S., 2017b. Geology, mineralization, and fluid inclusion characteristics of the Lermontovskoe reduced-type tungsten (± Cu, Au, Bi) skarn deposit, Sikhote-Alin, Russia. Ore Geol. Rev. 89, 15–39.
Soloviev, Serguei G., Kryazhev, Sergey G., Dvurechenskaya, Svetlana S., 2019. Geology, mineralization, and fluid inclusion characteristics of the Meliksu reduced tungsten skarn deposit, Alai Tien Shan, Kyrgyzstan: Insights into conditions of formation and regional links to gold mineralization. Ore Geol. Rev. 111, 103003. https://doi.org/10.1016/j.oregeorev.2019.103003.
Sun, S.-S., McDonough, W.F., 1989. Chemical and isotopic systematics of oceanic basalts: Implications for mantle composition and processes. Geol. Soc. London Spec. Publ. 42, 313–345.
Taylor, B.E., Liou, J.G., 1978. The low-temperature stability of andradite in C-O-H fluids. Amer. Miner. 63, 378–393.
Thiery, R., Kerkhof, A.M., Dubessy, J., 1994. νX properties of CH_4-CO_2 and CO_2-N_2 fluid inclusions: modeling for $T < 31$ °C and $P < 400$ bars. Eur. J. Mineral. 6, 753–771.
Thompson, J.F.H., Sillitoe, R.H., Baker, T., Lang, J.R., Mortensen, J.K., 1999. Intrusion-related gold deposits associated with tungsten-tin provinces. Miner. Deposita 34, 323–334.
Tooth, B., Brugger, J., Ciobanu, C., Liu, W., 2008. Modeling of gold scavenging by bismuth melts coexisting with hydrothermal fluids. Geology 36, 815–818.
Vikent'eva, O.V., Yu, Prokofiev V., Gamyanin, G.N., Goryachev, N.A., Bortnikov, N.S., 2018. Intrusion-related gold-bismuth deposits of North-East Russia: PTX parameters and sources of hydrothermal fluids. Ore Geol. Rev. 102, 240–259.
Volkov, A.V., Egorov, V.N., Sidorov, A.A., Alexeev, V.Y., 2010. Suites of auriferous dikes in the Yana-Kolyma belt. In: Tectonics and Geodynamics of Folded Belts and Platforms Proc. 12th Russian Tectonic Meeting, pp. 120–124 (in Russian).
Volkov, A.V., Savva, N.E., Sidorov, A.A., 2007. Plutonogenic deposits of fine-dispersed gold in the Russian Northeast. Doklady Earth Sci. 412 (1), 76–80.
Voroshin, S.V., Tyukova, E.E., Newberry, R.J., Layer, P.W., 2014. Orogenic gold and rare metal deposits of the Upper Kolyma District, Northeastern Russia: Relation to igneous rocks, timing, and metal assemblages. Ore Geol. Rev. 62, 1–24.
Wilkinson, J., Chang, Z., Cooke, D., Baker, M., Wilkinson, C., Inglis, S., Chen, H., Gemmell Jr., B., 2015. The chlorite proximator: a new tool for detecting porphyry ore deposits. J. Geochem. Explor. 152, 10–26.
Wood, S.A., Samson, I.M., 2000. The hydrothermal geochemistry of tungsten in granitoid environments: I. Relative solubilities of ferberite and scheelite as a function of T, P, pH, and mNaCl. Econ. Geol. 95, 143–182.
Yakubchuk, A.S., 2009. Revised Mesozoic-Cenozoic orogenic architecture and gold metallogeny in northern Circum-Pacific. Ore Geol. Rev. 35, 447–454.
Yuvan J., 2006. Fluid inclusion and oxygen isotope studies of high-grade quartz-scheelite veins, CanTung mine, Northwest Territories, Canada: products of late-stage magmatic-hydrothermal event. M.Sc. Thesis, Univ Missouri-Columbia. 105 p.
Zharikov V.A., 1970. Skarns. Internat. Geol. Rev. 12, 541-559, 619-647, 720-775.